

**A novel way to determine crack tip stress field
parameters involving displacement field estimated
using digital image correlation technique**

Harilal R

A Thesis Submitted to
Indian Institute of Technology Hyderabad
In Partial Fulfillment of the Requirements for
The Degree of Master of Technology



भारतीय प्रौद्योगिकी संस्थान हैदराबाद
Indian Institute of Technology Hyderabad

Department of Mechanical Engineering

June 2015

Declaration

I declare that this written submission represents my ideas in my own words, and where ideas or words of others have been included, I have adequately cited and referenced the original sources. I also declare that I have adhered to all principles of academic honesty and integrity and have not misrepresented or fabricated or falsified any idea/data/fact/source in my submission. I understand that any violation of the above will be a cause for disciplinary action by the Institute and can also evoke penal action from the sources that have thus not been properly cited, or from whom proper permission has not been taken when needed.



(Signature)

HARILAL R.

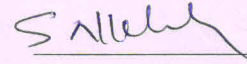
(Harilal R)

ME10B14M000003

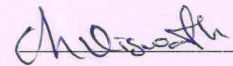
(Roll No.)

Approval Sheet

This Thesis entitled A novel way to determine crack tip stress field parameters involving displacement field estimated using digital image correlation technique by Harilal R is approved for the degree of Master of Technology from IIT Hyderabad



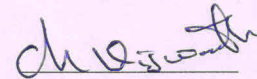
(Dr. Syed Nizamuddin Khaderi) Examiner
Dept. of Mechanical and Aerospace Engineering
IITH



(Dr. Viswanath Chinthapenta) Examiner
Dept. of Mechanical and Aerospace Engineering
IITH



(Dr. M. Ramji) Adviser
Dept. of Mechanical and Aerospace Engineering
IITH



(on behalf of Dr. C. P. Vyasarayani) Co-Adviser
Dept. of Mechanical and Aerospace Engineering
IITH



(Dr. S. Suriya Prakash) Chairman
Dept. of Civil Engineering
IITH

Acknowledgements

Though only my name appears on the cover of this Thesis, a great many people have conducted to its making. I owe my gratitude to all those people who have made this dissertation possible and because of whom my graduate experience has been one that I will cherish forever.

Foremost, I would like to express my sincere gratitude to my advisor Dr. M. Ramji for the continuous support of my Masters study and research, for his patience, motivation and immense knowledge. I am fortunate to have an advisor who gave me the freedom to explore on my own, and at the same time guided me when my steps stumbled.

I would like to extend my heartfelt thanks to Dr. C P Vyasarayani. His patience and support helped me overcome many crisis situations and finish this dissertation. I am deeply grateful to him for the long discussions that helped me to sort out the technical difficulties of my work.

I would like to thank Justin Blaber from Georgia Institute of Technology for his valuable suggestions in the field of software development. He was always available through mail for clearing my doubts and providing new insights.

I would like to thank Mr Mohammad Kashfuddoja and Mr Naresh Reddy for their valuable suggestions and aid in performing tensile and compression tests which helped me to finish my research work on time. I am thankful to all my colleagues at Engineering Optics Lab, Mr Saranath K M, Mr Yagnik Kalariya, Mr Pratap Rao Patil, Mr Milind Talele, Mr Yogesh Wagh, Mr Anup Teejo Mathew and Mr Atul Gavade for their constant support in completion of this thesis. I would extend my thanks to all the staff of central workshop for their assistance in specimen preparation and material management. Most importantly, none of this would have been possible without the love and support from my family. My family to whom this thesis is dedicated to, has been a constant source of love and concern.

Dedication

Dedicated to my family and teachers

Abstract

In the present work, an experimental study is carried out to estimate the mixed-mode stress intensity factors (SIF) for different cracked specimen configurations using digital image correlation (DIC) technique. For the estimation of mixed-mode SIFs using DIC, a new algorithm is proposed for the extraction of crack tip location and coefficients in the multi parameter displacement field equations. The required displacement data surrounding the crack tip has been obtained using 2D-DIC technique. An open source 2D DIC software Ncorr is used for the displacement field extraction. To compare its capabilities with the existing commercial code, various experiments are conducted and results have been compared with commercial software Vic 2D. There is good coherence in results obtained from both the software. An additional SIF estimation module has been developed in MATLAB for SIF estimation from the displacement data obtained from Ncorr open source 2D DIC software. The presented methodology has been used to extract SIF's for specimen configurations like single edge notch (SEN) specimen and center slant crack (CSC) specimens made out of Al-2014 T6 alloy. The experimental results have been compared with the analytical values and they are found to be in good agreement, thereby confirming the accuracy of the algorithm being proposed. As an additional visual confirmation, the experimental displacement contours are superimposed over the theoretically reconstructed displacement contours obtained using extracted crack tip parameters. They are found to be in coherence with each other. Further, the same algorithm has been intelligently extended to fatigue crack growth study as well. Two types of specimens namely, un-repaired and single sided carbon fiber reinforced polymer (CFRP) patch repaired cracked aluminium panel under fatigue loading are considered. The mixed mode SIFs are estimated from the displacement field data at various crack lengths and they are compared with their finite element analysis (FEA) estimates based on a previous study. The numerical and experimental SIFs are found to be in coherence with each other.

Contents

Declaration	ii
Approval Sheet	iii
Acknowledgements	iv
Abstract	vi
Nomenclature	viii
1 Introduction and Literature Review	1
1.1 Introduction	1
1.1.1 Stress Intensity Factor	1
1.1.2 Introduction to Digital Image Correlation	2
1.2 Literature Review	3
1.3 Scope and Motivation	5
1.4 Thesis Layout	6
2 Adaptation of Open Source Ncorr Software for Solid Mechanics Applications	7
2.1 Introduction	7
2.2 Specimen Geometry and Experimental Set Up	8
2.3 Experimental Procedure	9
2.4 Results and Discussion	10
2.4.1 Epoxy Ring under Diametral Compression	10
2.4.2 Beam under four point loading	15
2.5 Smoothing algorithm implementation in Ncorr	18
2.5.1 Boundary Encoding	19
2.5.2 Experimental Data Acquisition and Processing	20
2.5.3 Smoothing Using Mean Absolute Deviation	20
2.5.4 Smoothing Using Median Absolute Deviation	21
2.6 Closure	22
3 SIF Estimation in SEN and CSC specimen under static loading	24
3.1 Introduction	24
3.2 Test procedure and Specimen fabrication	25
3.3 Experimental estimation of SIF	26
3.3.1 Multi-parameter displacement field equations	27
3.3.2 Solution Procedure	27

3.4	Results and Discussions	30
3.4.1	Experimental determination of SIF for SEN specimen	30
3.4.2	Experimental determination of SIF for CSC specimen	32
3.5	Closure	36
4	Fatigue crack growth study in a CFRP patch repaired Al2014-T6 panel having an inclined crack involving DIC technique	37
4.1	Introduction	37
4.2	Geometry and specimen preparation	38
4.3	Experimental setup	39
4.4	Experimental SIF evaluation	40
4.4.1	Multi-parameter displacement field equations	40
4.4.2	Solution Procedure	41
4.5	Finite Element Modeling	45
4.6	Results and Discussions	46
4.6.1	Unrepaired Panel	46
4.6.2	Single Sided Repaired Panel	47
4.7	Closure	48
5	Conclusions and Recommendations	49
	References	50

Chapter 1

Introduction and Literature Review

1.1 Introduction

1.1.1 Stress Intensity Factor

For the safe operation of aircraft components, damage tolerance analysis is necessary. Continuous maintenance at regular intervals are required for an aircraft for its satisfactory performance and safe flight. Stress Intensity factor (K) is a fundamental parameter to determine the crack growth life as well as critical crack length in aircraft components. The general equation for stress intensity factor can be expressed as

$$K = \sigma\beta\sqrt{\pi a} \quad (1.1)$$

Here σ is the far field stress, a is the crack length and β is a parameter accounting for geometry effects. The value of β for common specimen configurations are available in reference [1].

There are three linearly independent cracking modes used in fracture mechanics. These loading configurations are classified as mode I , mode II and mode III as shown in Figs. 1.1(a) ,1.1(b) and 1.1(c) respectively. In mode I or opening mode, the crack surfaces directly move apart. In Mode II or sliding mode, the crack surfaces slide over one another in a direction perpendicular to the leading edge of the crack. In mode III or tearing mode, the crack surfaces move relative to one another and parallel to the leading edge of the crack. The most commonly found mode of loading in engineering problems is mode I. The stress intensity in any mode situation is directly proportional to the applied load on the material. Failure studies focus more on brittle fracture since it can occur rapidly without any warning. Brittle fractures take place when the applied stress increases such that the stress state at the crack tip reaches a critical value. The linear-elastic fracture toughness of a material is determined from the stress intensity factor at which crack propagation in the material is initiated. If a very sharp crack can be made in a material, the minimum value of K_I can be empirically determined, which is the critical value of stress intensity required to propagate the crack. This critical value determined for mode I loading is referred to as the critical fracture toughness K_{Ic} of the material. It is expressed in $\text{MPa}\sqrt{m}$.

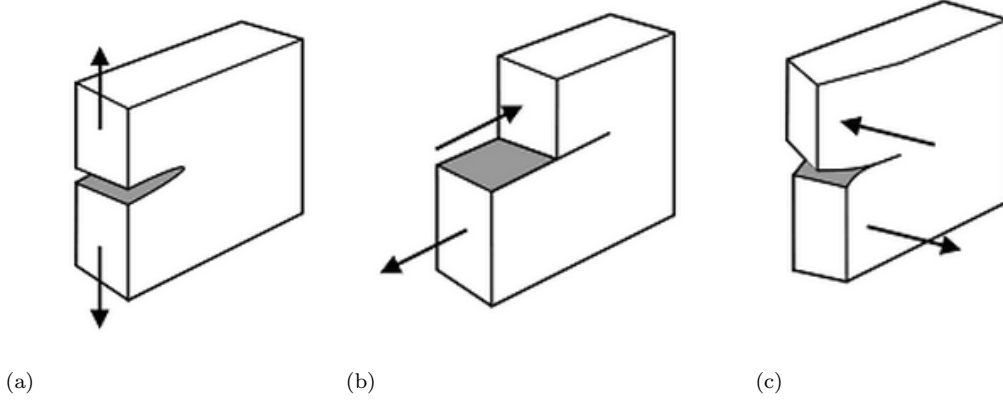


Figure 1.1: Modes of loading (a) mode I (b) mode II (c) mode III

1.1.2 Introduction to Digital Image Correlation

Digital image correlation is a widely used non-contact whole field surface displacement and strain measurement technique that came into popularity beginning from the 1980s [2, 3]. The technique uses artificial or natural speckle pattern to track the motion of the reference subsets of the images captured in the un-deformed configuration and locate them in the deformed configuration. For estimating displacements, a correlation criterion is used in evaluating the similarity between the reference and deformed subsets. Along with the correlation criterion coupled with optimization algorithms, the location of the subset is identified in the deformed image by comparing the intensity pattern of the reference subset. A widely used correlation criterion is ZNCC [4] as shown in Eq. 1.2

$$C_{ZNCC} = \frac{\sum_{i=-M}^M \sum_{j=-M}^M [f(x_i, y_j) - f_m][g(x'_i, y'_j) - g_m]}{\sqrt{\sum_{i=-M}^M \sum_{j=-M}^M [f(x_i, y_j) - f_m]^2} \sqrt{\sum_{i=-M}^M \sum_{j=-M}^M [g(x'_i, y'_j) - g_m]^2}} \quad (1.2)$$

Here, $f(x, y)$ and $g(x', y')$ are the intensity values in the reference and deformed images. f_m and g_m are the mean intensity values of the subsets in the un-deformed and deformed configurations. M is the width of subset in pixels. The x' and y' coordinates in Eq. 1.2 can be expanded as shown below

$$x' = x + u + \frac{\partial u}{\partial x} dx + \frac{\partial u}{\partial y} dy \quad (1.3)$$

$$y' = y + v + \frac{\partial v}{\partial x} dx + \frac{\partial v}{\partial y} dy \quad (1.4)$$

Here, u and v are translations of the centre of the subset along x and y directions. In case of 2D DIC technique, a single camera is used for capturing the images. The captured images are later processed using a 2D DIC software to obtain in-plane surface displacements and strains. 3D DIC technique is based on the principles of stereo vision and uses two CCD cameras to capture the images of the object from two different vantage points. The synchronization of the cameras are achieved through a detailed calibration process. Readers are advised to refer the following literature [4, 5, 6, 7] for an in depth understanding on the development and capabilities of DIC.

1.2 Literature Review

Many researchers have developed and applied methodologies for estimating SIF's involving different experimental techniques. These experimental techniques include whole field non-contact optical methods such as holographic interferometry [8], electronic-speckle-pattern interferometry (ESPI) [9], Moiré interferometry [9, 10], coherent gradient sensing [11], method of caustics [12], photoelasticity [13], digital image correlation [14] etc, as well as contact methods such as measurements using resistance strain gauges [15]. Ramesh *et al.* [16] developed a software based on the multi-parameter stress field equations proposed by Atluri and Kobayashi [17], by implementing the over deterministic least squares technique towards evaluation of mixed mode crack tip stress field parameters based on photoelastic data. However, photoelasticity is only suitable for transparent birefringent plastics. Methods like holography and other interferometric techniques are very sensitive to vibration and requires a coherent light source. Interferometric techniques measure the deformation by recording the phase difference of the scattered light wave from the specimen surface before and after deformation. The measurement results are often presented in the form of fringe patterns which requires further processing and phase analysis in order to extract the basic data. Non-interferometric techniques determine the surface deformation by comparing the gray intensity changes of the specimen before and after deformation, and generally have less stringent requirements under actual experimental conditions [18]. Yates *et al.* developed techniques for tracking the crack growth and the evaluation of the mixed mode crack tip stress fields using thermo-elasticity [19]. Recently, Sarangi *et al.* [20] proposed a methodology for accurate estimation of SIF's by optimising the strain gauge locations. They have suggested a new strain gauge based methodology for the experimental determination of the mixed mode SIF's (both K_I and K_{II}). T.C. Chu *et al.* developed a computer program based on DIC to estimate displacement components and deformation gradients of an object surface due to deformation. Several experiments were performed to demonstrate the viability of this correlation method in experimental mechanics [21].

Amongst these experimental techniques, digital image correlation (DIC) have become popular for SIF determination because of its relatively simple specimen preparation, ease of use and requirement of less complicated optics. Also it is truly a whole field technique and could be employed for any class of material. It requires specimen surface to be coated with artificial speckle pattern for estimation of displacement and strain fields. It provides information about the displacements and strains by comparing the digital images of the specimen surface coated with artificial speckle pattern in the un-deformed and deformed states respectively. In case of a 2D DIC setup, only one camera is used for the measurement of in-plane surface displacements and strains. Sutton *et al.* [7] employed 2D-DIC to study the three-dimensional effects near the crack-tip. In order to reduce the experimental noise, they used smoothed u -displacement and v -displacement field obtained for single edge notch specimen to predict the presence of three-dimensional and/or non-linear zone near the crack-tip. However, most of these studies were limited to mode-I crack problems. In 2008, Lopez-Crespo [22] *et al.* developed a generalised approach for determining K_I and K_{II} for a specimen having any mode mixity, directly from displacement fields obtained using DIC for crack growth problem under fatigue loading. The methodologies described in the literature either neglect the error introduced due to ambiguous location of the crack-tip or use non-linear iterative algorithm to locate the crack-tip [23, 24]. Using the whole field displacement data (u_x and u_y) obtained from 2D-DIC, Yoneyama *et al.* [14, 25] extended the non-linear least square algorithm which considered u_x and u_y displacement

components in a combined way. They proposed new convergence criteria based on the correlation coefficient and the sum of absolute values of error between experimentally obtained and theoretically reconstructed displacement fields.

Scientists have tried to reduce SIF in aircraft components by introducing patch repairs on cracked surfaces. In the early 1970s Baker *et al.* [26] introduced the repair of cracked aircraft structures made of aluminium using composite patch for enhancing their fatigue life. Bonded patch repairs can be applied single sided (asymmetric) or double sided (symmetric) on the cracked panel. Double sided patch work is more efficient in SIF reduction compared to the single sided patch. But often both sides of the cracked region may not be easily accessible for repairs which is why single sided patch is preferred. Jones [27] developed theoretical and design aspects for predicting the loss in efficiency due to single sided repair. Umamaheswar and Singh [28] used finite element method to study the behaviour of single sided patch repairs applied to thin aluminium sheets. They brought out the SIF variation through the thickness of the panel assuming a straight crack front. Chukwujekwu Okafor *et al.* [29] conducted both experimental and finite element based analysis for obtaining the stress distribution on cracked plates with single sided octagonal patch. They found that the zone of maximum stress shifted from the crack front (for cracked specimen) to the edge of the patch, due to the high peel stress developed at the patch overlay edge. The peel stresses in bonded joints normally peaks at the end of the overlap, which in turn can cause failure of the adhesive layer, thereby reducing the effectiveness of the repair. To avoid the severity of the peel stress occurring at the overlapping ends, Duong [30] suggested the usage of a tapered patch. Following the recommendation a tapered patch is being used in the present study. Researchers have carried out experimental investigations on repaired panels having mixed mode crack orientations. Ayatollahi and Hashemi [31, 32] used FEA to investigate the effect of composite patching on SIF reduction for an inclined center cracked panel under different mixed mode loading configurations. Recently, Ramji and Srilakshmi [33] studied the mechanics of single sided and double sided repair of an inclined center cracked panel using FEA. Ramji *et al.* [34] have investigated the influence of different patch shapes on the performance of the repair on the mixed mode panel. They found that extended octagonal patch shape performs better in reducing SIF at the crack tip.

In 2009, Poissant and Barthelat [35] introduced a subset splitting algorithm for the effective application of digital image correlation on discontinuous displacement fields. They proposed a novel approach which enables the subset to split into two sections when a discontinuity is detected. Recently Ronghua Zhu *et al.* [36] investigated the registration accuracies of several subset shapes and control point locations used in DIC technique. They found that the varying the subset shapes affect the registration accuracy while varying the control points have little impact. With the help of these findings, they developed a non central algorithm for whole field deformation measurement. Jinlong Chen *et al.* [37] presented an improved extended digital image correlation technique to measure discontinuous deformation across the crack. They proposed a non rectangular subset to eliminate the effect of crack width on measurement accuracy. Reng-cai Yang [38] developed a regularized finite-element digital image correlation technique to solve the displacement field with fine and irregular structure. He proposed an algorithm which is capable of resolving displacement field with very fine structure at reasonable accuracy. Ge Yang *et al.* [39] experimentally investigated the damage mechanisms in granites under uniaxial tension. They have used DIC for displacement and surface strain measurement. M. Eskandari *et al.* [40] studied the effect of deformation temperature on the

strain localization during tensile loading of micro alloyed steel using an adapted DIC technique.

Hosseini Toudeshky *et al.* [41, 42] studied fatigue crack growth in single side repaired thick and thin aluminium panels having inclined cracks with different lay-up configuration and patch thickness. Srilakshmi *et al.* [43] investigated crack growth in composite patch repaired aluminium panels using FEA and DIC under fatigue loading. They observed that the fatigue life of double-sided repaired panel is twice that of single-sided repaired panel configuration. Seo and Lee [44] numerically and experimentally investigated the fatigue crack growth (FCG) behaviour of thick cracked panels repaired with single sided composite FRP patch. They studied panel configurations with both skewed and uniform crack front for the fatigue life estimation using FEA. They found that, for the single-sided repairs, skewed crack front model predicted the fatigue life more accurately in comparison with the experiments. Lee and Lee [45] performed numerical and experimental studies on the FCG behaviour of aluminium plate with straight crack, repaired using a single sided composite patch. The single sided repair was found to be more effective for thin plates compared to thicker ones. Tsai and Chen [46] conducted experimental and numerical study on single sided Boron FRP patch repaired aluminium panels. Tay et al. [47] performed experiments on an aluminum panel with a cracked bolt hole repaired using Boron FRP patch. They observed that the patched specimens with the press-fitting plugs lasted longer than the notched specimens with very less crack growth. Schubbe and Mall [48] have carried out the experimental analysis on the FCG behavior of both thick and thin single sided patch repaired aluminum panels. They conducted a parametric study by varying the stiffness ratio as well as patch length. They found that the patch length does not influence the fatigue life of the repaired thick panel. Further, they observed that the increase in the stiffness ratio of patch to panel enhanced the fatigue life of repaired panels.

1.3 Scope and Motivation

The estimation of stress intensity factor for a given crack or component geometry is a critical input for service life estimation in damage tolerant based design approach. Analytical solutions are available for finding SIF for various simple specimen geometries and loading configurations. For complex configurations, SIF needs to be extracted either by experiment or by numerical analysis. Scientists have used several optical methods like holographic interferometry, Moire interferometry and photoelasticity for SIF estimation. Methods like holography and other interferometric techniques are very sensitive to vibration and requires a coherent light source, while photoelasticity is only suitable for transparent birefringent plastics. Among the whole field measurement techniques, Digital image correlation (DIC) have become popular for SIF determination because of its relatively simple specimen preparation, ease of use and requirement of less complicated optics. DIC technique is used for estimating surface displacements and strains on the specimen surface. The existing methods for SIF estimation from displacement field requires manual data collection around the crack tip. These methods are highly sensitive to the initial crack tip location. Existing methods use non-linear least square algorithm to minimize the objective function, using which one often finds the local minimum leading to a bad curve fit to the experimental data. An algorithm to obtain the global minimum of the objective function and faster convergence is to be developed. The same methodology can be extended to fatigue as well.

1.4 Thesis Layout

Chapter 1 is about introduction, literature review, scope and motivation in the area of stress intensity factor estimation. It includes a brief introduction about the technique of digital image correlation which is extensively used for surface displacement measurements in the present work.

Chapter 2 validates the accuracy of the open source 2D DIC software Ncorr. Various experiments like ring under diametral compression and beam under four point loading are conducted and the results are compared with the results obtained from commercially available DIC software VIC 2D. A displacement smoothing algorithm implementation in Ncorr is also presented.

Chapter 3 discuss the implementation of a new algorithm for estimation of mixed mode SIFs from displacement field obtained using DIC technique under static loading case.

Chapter 4 extends the same algorithm developed in the previous chapter to fatigue crack growth experiments. SIF estimation in un-repaired and single sided CFRP patch repaired panels are presented.

Chapter 5 concludes the thesis with recommendations for future work.

Chapter 2

Adaptation of Open Source Ncorr Software for Solid Mechanics Applications

2.1 Introduction

There are various contact and non-contact techniques in the field of experimental mechanics for measurement of surface deformation and strain. Direct measurement techniques like strain gauge method and non-contact methods like Moire interferometry [49], Holography [50], Speckle interferometry [51] and Digital Image Correlation (DIC) are among the most popular ones. Among these methods, the interferometric techniques have stringent requirements like vibration free setup and coherent light source. The relatively simple optics and less stringent requirements gives DIC an edge over other conventional methods. Digital image correlation has been extensively used for displacement and strain field estimation in various applications like material characterization, structural health monitoring, fatigue crack growth, high temperature testing etc. With the advancement in computational capabilities, more robust algorithms have emerged for tracking the material points to estimate whole field displacements and strains. The adaptability of DIC technique helps in exploiting the advancements in image capturing technology enabled in microscopes and high speed cameras to estimate displacement and strain data from the acquired images.

There are various commercial software available in the market which uses 2D-DIC as a tool to estimate surface displacement and strain fields. Correlated Solutions, Dantec Dynamics are quite a few well known software companies producing 2D DIC software which are known for their accuracy and user friendliness. A lot of investments are involved in procuring these commercial software along with additional costs for their version upgrades. The limitations of using commercial software are the inherent costs involved in procuring and the restrictions imposed on users, as they cannot modify the source code as per their requirements. Alternatively, an open source, user friendly software can drastically cut down costs and could be modified as per user requirements. Ncorr [52] is one such open source 2D DIC code based on MATLAB [53] and developed at Georgia Institute of Technology by Antonia Antonious group. It is capable of estimating surface displacement and strain fields from

the given input speckle images. To compare its capabilities with the existing commercial code, various experiments are conducted and results have been compared with commercial software Vic 2D, developed and sold by correlated solutions Inc, USA.

The following study compares the surface displacements and strain fields generated by Ncorr and Vic 2D using experimental input speckle images acquired from different experiments like ring under diametral compression and beam under four point loading. The comparison helps in bolstering the credibility of Ncorr as a reliable open source DIC tool thereby making it a critical part of low cost DIC system for solid mechanics research studies.

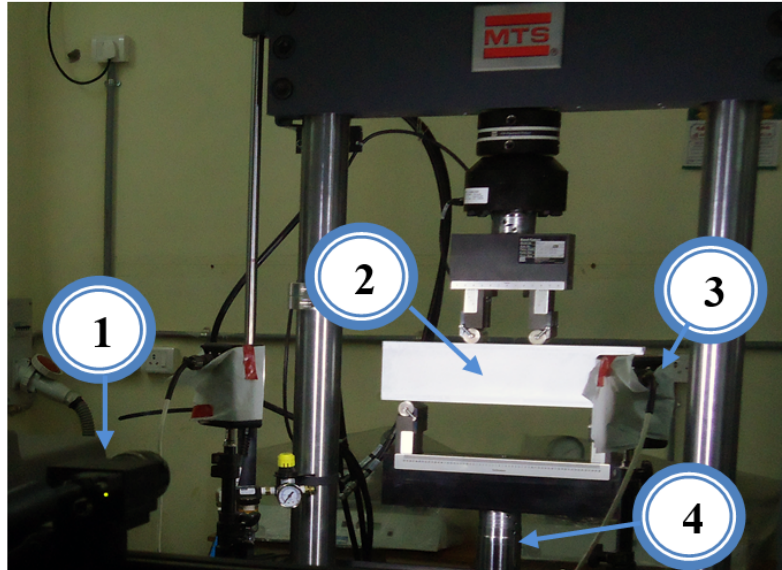
2.2 Specimen Geometry and Experimental Set Up

The ring and beam specimens are cut from an epoxy sheet of 6 mm thickness casted in house by mixing commercially available C51 epoxy resin and K6 hardener in the proportion of 10:1 by weight. The mixture is mixed at room temperature for about 30 minutes with due precaution taken to avoid the formation of any air bubbles. The resin-hardener mixture is then poured into the mold and left to cure for 24 hours at room temperature. A circular ring with outer and inner radii 80 mm and 40 mm respectively and a rectangular beam of length 220 mm and breadth 40 mm are milled from the 6mm casted epoxy sheet. The material properties of the epoxy sheet used is as specified in Table 2.1.

Table 2.1: Material properties of the specimens used

Material	Yield Strength	Young's Modulus	Poisson's ratio
Epoxy	35 MPa	3300 MPa	0.37

The surfaces of the specimens are coated with thin layer of white acrylic paint. Using an airbrush, carbon black paint is sprayed over the white surfaces, creating random black and white artificial speckle pattern. The 2D DIC optical system consists of a CCD camera with a spatial resolution of 2448 x 2048 pixels. Camera is aligned parallel to the specimen surface in order to eliminate errors due to out of plane displacements. A Tamron lens with 180 mm focal length is mounted on the camera and is then connected to a computer controlled image acquisition system. LED flood lights are used to ensure adequate image contrast. A computer controlled MTS Landmark servo hydraulic cyclic testing machine is used to apply the specified load onto the specimens. The experimental setup used for beam under four point bending is shown in Fig. 2.1. Similar to the shown setup, the diametral load on the ring is applied by replacing the four point bending fixture with compression platens in MTS servo hydraulic system.



- | | |
|---------------|---------------------|
| 1. CCD Camera | 3. LED Light Source |
| 2. Specimen | 4. Actuator |

Figure 2.1: 2D DIC Experimental set up for beam under four point bending.

2.3 Experimental Procedure

The ring is arrested at the top and a diametral compressive load of 1kN is applied at the bottom of the epoxy ring using compression platens attached to the MTS landmark servo hydraulic system. Sequences of images are collected as the loading progresses from 0 to 1kN. The epoxy beam is subjected to a four point bend test with loading point separations of 120 mm in the top surface and 180 mm in the bottom surface as shown in Fig. 2.12(a). A compressive load of 1kN is applied at the bottom surface of the beam at the two load points P and Q as shown in Fig. 2.12(a). The images collected during the experiments are then processed using Ncorr and Vic 2D to estimate the displacement and strain fields. For computing displacements using DIC, a subset is chosen from the reference image and its corresponding location is tracked in the deformed image [4]. The square subset size and step size used in Vic 2D for the analysis is 21 x 21 and 5 respectively. Ncorr is equipped with circular subset and its radius is set to 11 with a subset spacing of 5. Ncorr uses the Inverse Compositional Gauss-Newton (IC-GN) [5] nonlinear solver which is fast, robust and accurate in displacement measurement compared to classical Newton Raphson or Forward Additive schemes. The displacement gradients or strains can be directly calculated using Newton Raphson (NR), Quasi NR, LevenbergMarquart algorithm (LM) [54] or Genetic algorithm. The error in estimated strain fields using NR or genetic method is of higher order and limits its use only for strain values approximately greater than 0.010 [6]. Another approach is to use numerical differentiation to derive strains from displacement field. Eliminating the noise from the displacement data prior to strain calculation can improve accuracy in computed strains. For strain calculation, Ncorr uses a least squares plane fit to a contiguous circular group of displacement values. The radius is set to 3 pixels prior to strain computation.

2.4 Results and Discussion

2.4.1 Epoxy Ring under Diametral Compression

For validation of the experiment, a finite element model of the ring is created using 2D, 6 node triangular plane 183 element and the boundary conditions are applied as per the experimental loading conditions. The ring is arrested at the top and a point load of 1kN is applied at the bottom, simulating the testing conditions. The displacement contours (u, v) obtained from the finite element model of the ring is shown in Fig. 2.2. During the DIC analysis, the same set of images grabbed during the diametral compression of the ring is given as the input for both Ncorr and Vic 2D for computing displacements and strains. The u displacement contours from Ncorr and Vic 2D for the ring problem is shown in Fig. 2.3. Due to symmetry of the specimen and the loading configuration, only half section of the loaded ring is shown in Fig. 2.3. To examine the results more closely, the displacement and strain values are plotted along a line AB as shown in Fig. 2.3. Fig. 2.4 and Fig. 2.6 shows the comparison of u and v data obtained along line AB obtained from the Ncorr and Vic 2D for the same set of input images. The u and v displacement contours obtained from Finite Element Analysis (FEA) is compared with DIC prediction. They are in good coherence with each other as shown in Figs. 2.2, 2.3 and 2.5

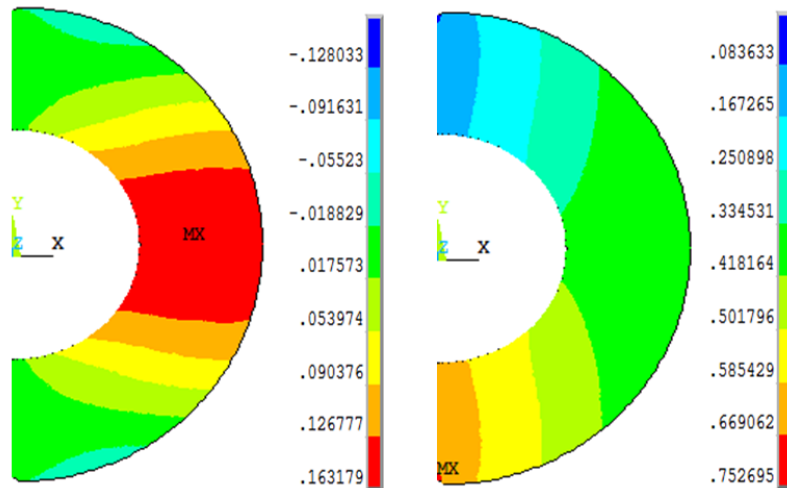


Figure 2.2: u displacement contours (left) and v displacement contours (right) for the ring under diametral compression obtained using FEA. (All values in *mm*)

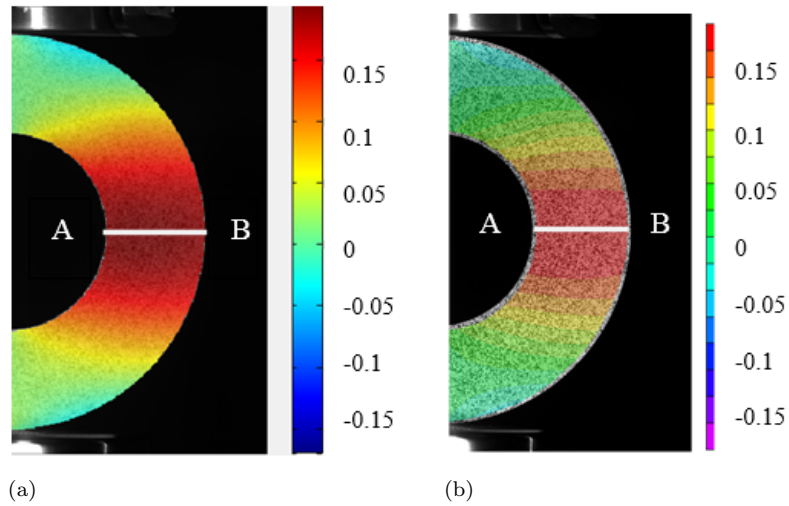


Figure 2.3: u displacement contours for the ring under diametral compression obtained from DIC technique (All values in mm) (a) From Ncorr (b) From Vic 2D

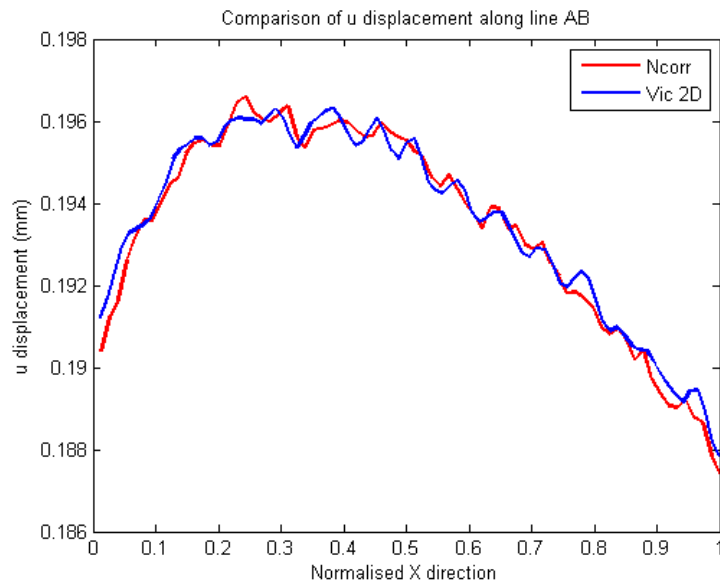


Figure 2.4: Comparison of u displacement along the line AB between Ncorr and Vic 2D estimates

There is a slight deviation between Ncorr and Vic 2D in estimating u displacement along line AB. This deviation can arise due to the difference in subset shape being used in the software. The y axis in Ncorr is positive downwards while in Vic 2D the y axis is positive upwards. This results in a sign change in representation of v displacement as shown in Fig. 2.5. The magnitude of the v displacements along the line AB are compared in Fig. 2.6. The field seems to be similar and it contains lot of undulations.

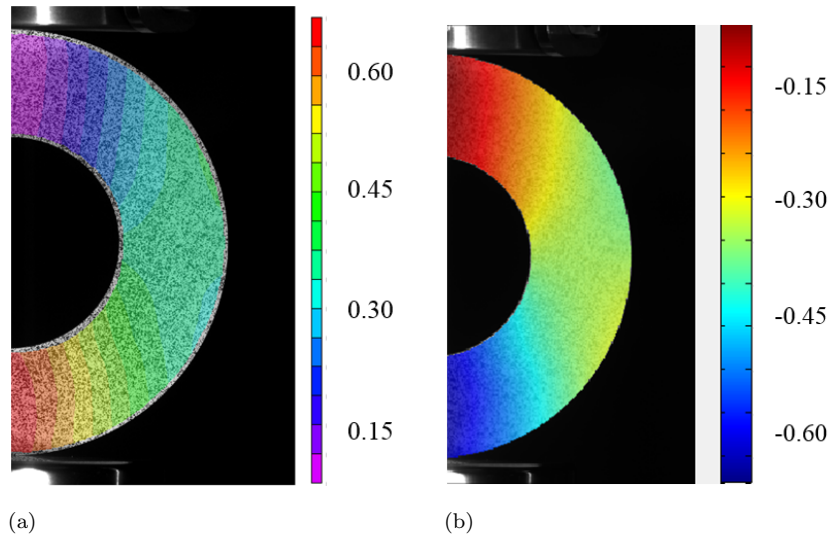


Figure 2.5: v displacement contours for the ring under diametral compression obtained from DIC technique. (All values in mm) (a) From Ncorr (b) From Vic 2D

The accuracy of the strains computed from numerical differentiation is influenced by the noise contained in the displacement field. Also, for the ring problem, the orders of magnitude of the computed strains are very small. These factors can cause slight deviation in the strains computed by Ncorr and Vic 2D. The sensitivity towards noise is also dependent on the numerical schemes used for strain computation in Ncorr and Vic 2D. The ϵ_{xx} , ϵ_{yy} and ϵ_{xy} contours obtained using DIC technique is shown in Figs. 2.7, 2.9 and 2.11. Further comparison of the ϵ_{xx} and ϵ_{yy} strain values from both softwares along line AB is shown in Figs. 2.8 and 2.10.

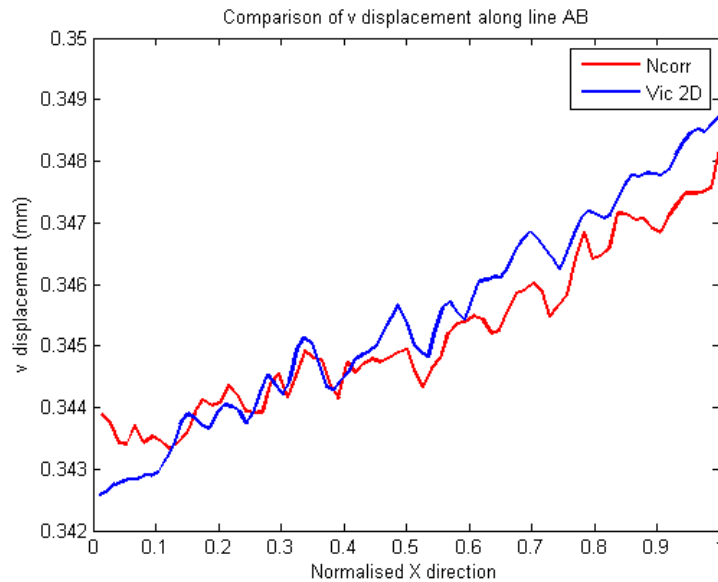


Figure 2.6: Comparison of v displacement along the line AB between Ncorr and Vic 2D estimates

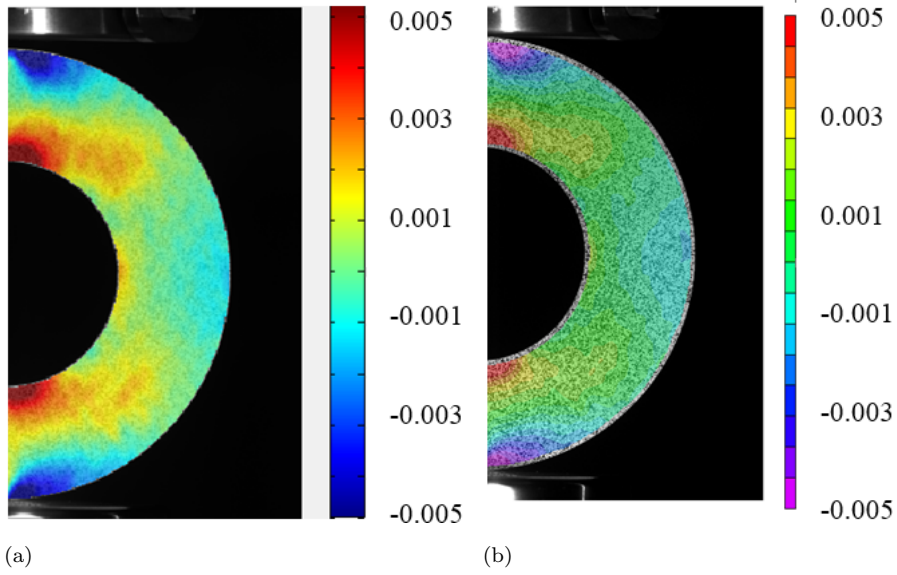


Figure 2.7: ϵ_{xx} contours obtained for an epoxy ring under a diametral load of 1 kN using (a) Ncorr (b) Vic 2D

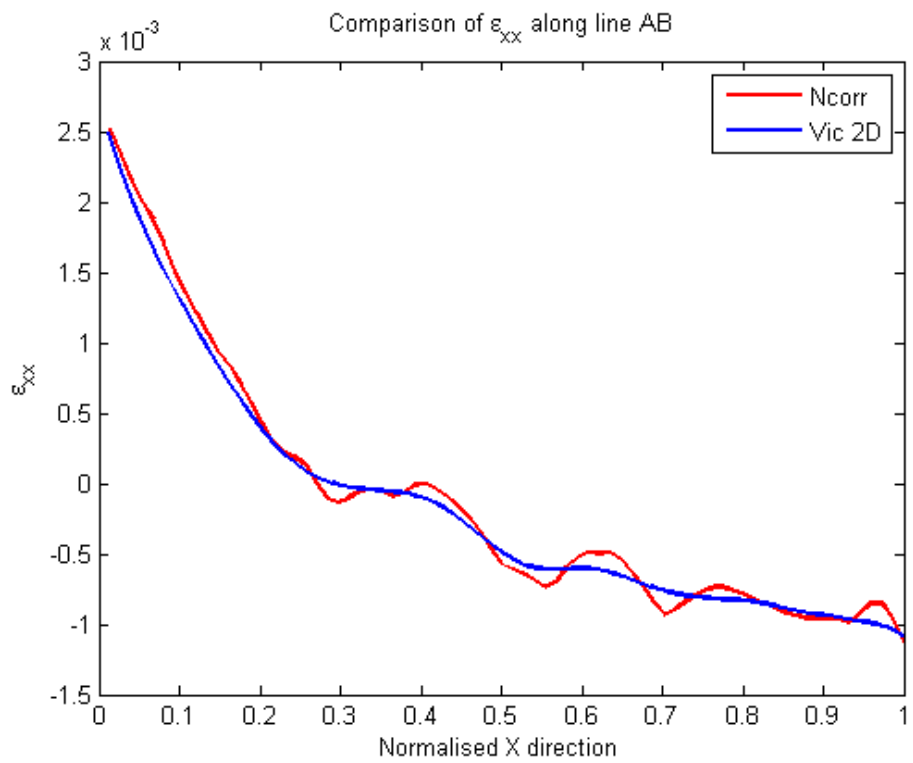


Figure 2.8: Comparison of ϵ_{xx} along the line AB between Ncorr and Vic 2D estimates

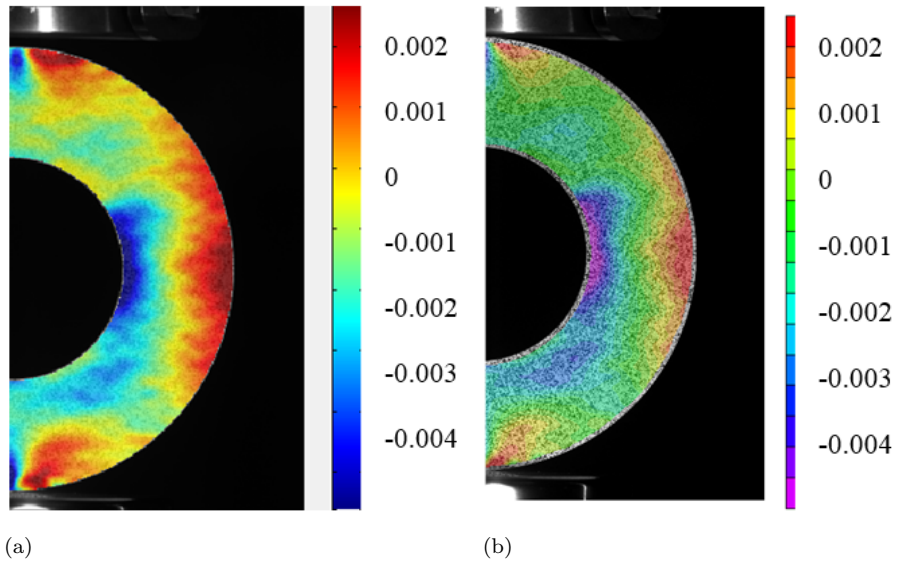


Figure 2.9: ϵ_{yy} contours obtained for an epoxy ring under a diametral load of 1 kN using (a) Ncorr (b) Vic 2D

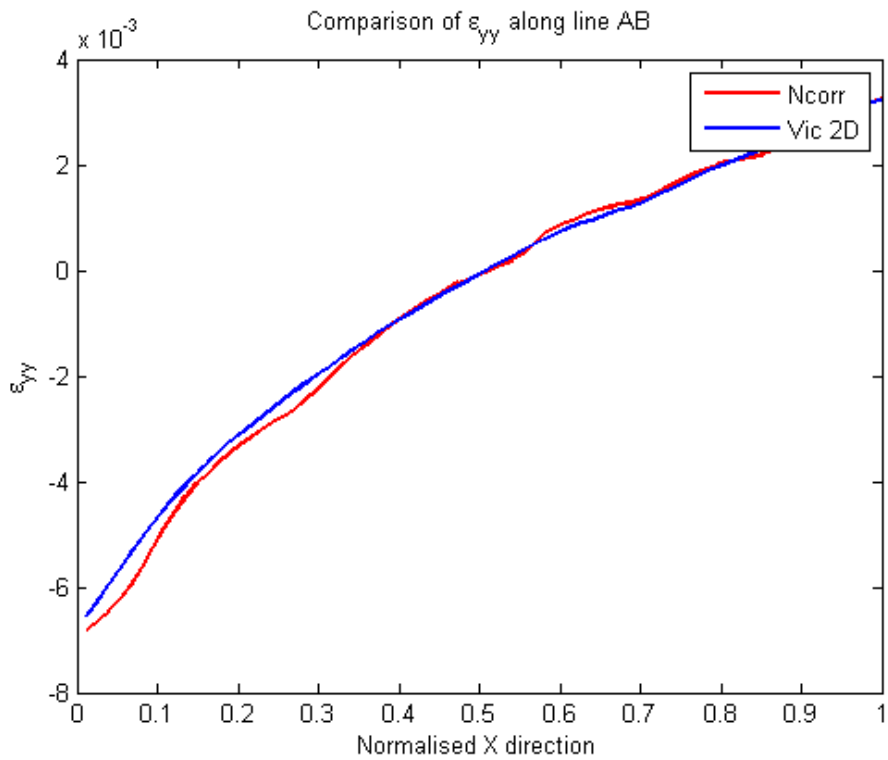


Figure 2.10: Comparison of ϵ_{yy} along the line AB between Ncorr and Vic 2D estimates

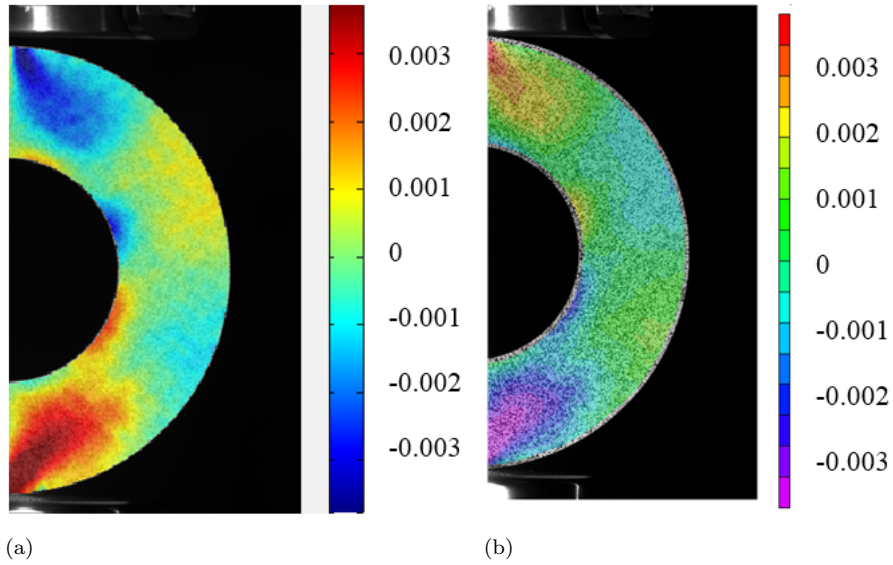


Figure 2.11: ϵ_{xy} contours obtained for an epoxy ring under a diametral load of 1 kN using (a) Ncorr (b) Vic 2D

2.4.2 Beam under four point loading

The epoxy beam is kept in four point bend configuration under a 1 kN load applied from bottom. The u displacement contours of the epoxy beam under the prescribed loading obtained from Ncorr is shown in Fig. 2.12(a). Fig. 2.12(b) shows the corresponding u displacement contours from Vic 2D. For further comparison, a line CD is drawn as shown in Fig. 2.12 and the corresponding displacement and strain values obtained from the two software are compared.

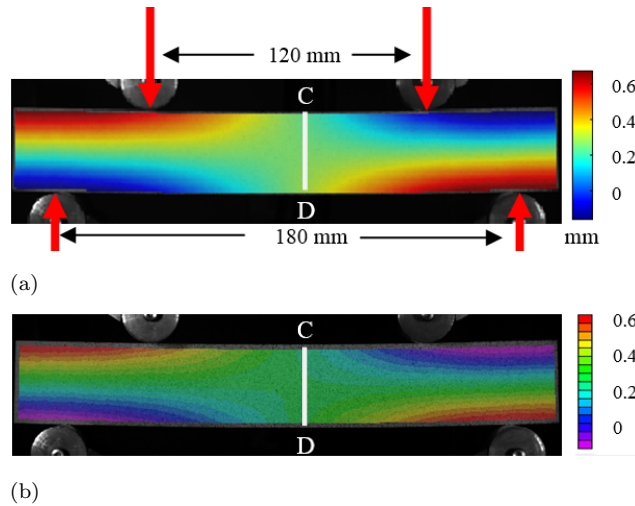


Figure 2.12: u displacement contours for an epoxy beam under four point bending using (a) Ncorr (b) Vic 2D

The v displacement contour for the same problem is shown in Fig. 2.13. Qualitatively both of them compare well. The sign change is caused due to the difference in the y axis orientation.

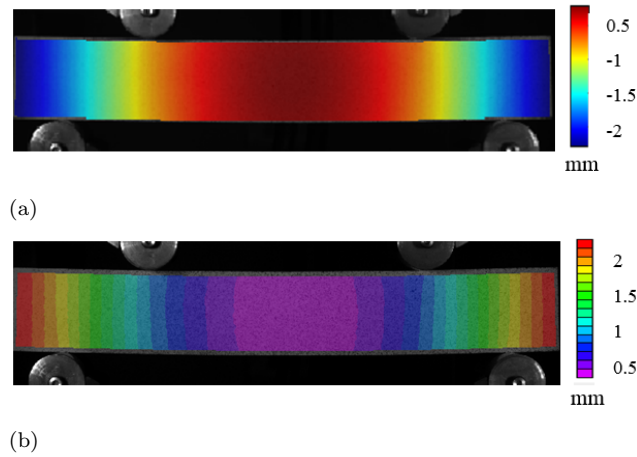


Figure 2.13: v displacement contours for an epoxy beam under four point bending using (a) Ncorr (b) Vic 2D

Figs. 2.14 and 2.15 show the comparison of u and v displacement data obtained from Ncorr and Vic 2D along the line CD. Figs. 2.16(a) and 2.16(b) show the xx contour obtained using Ncorr and Vic 2D for the same specimen at the same load. Fig. 2.18 shows the yy contour obtained from both softwares. The displacement and strain values along the line CD is found to be in good agreement with each other. Fig. 2.17 shows the quantitative comparison of ϵ_{xx} along the line CD obtained from both Ncorr and Vic 2D. They agree very well, thereby confirming the accuracy of Ncorr software. Similarly yy data along the line CD is compared in Fig. 2.19. Both data are in good coherence.

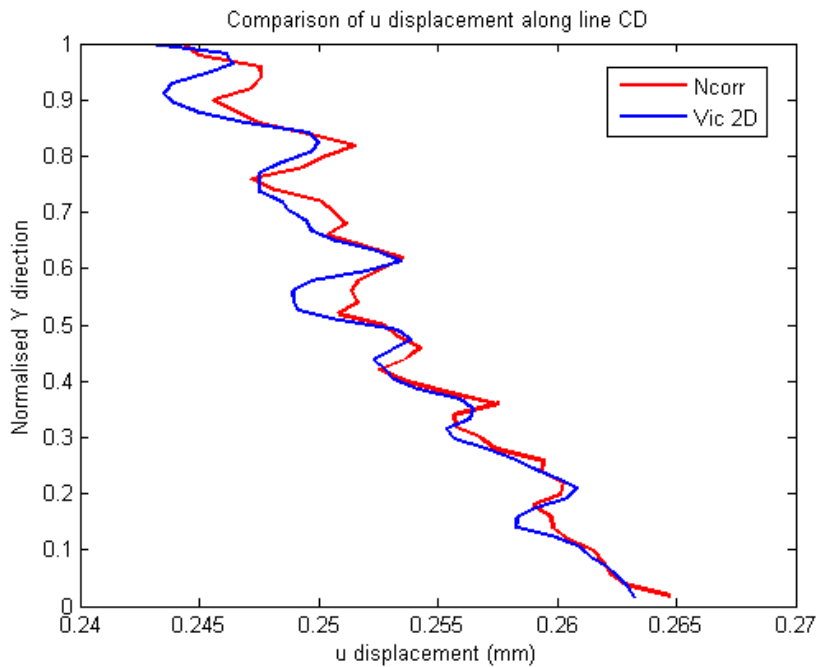


Figure 2.14: Comparison of u displacement along the line CD between Ncorr and Vic 2D estimates

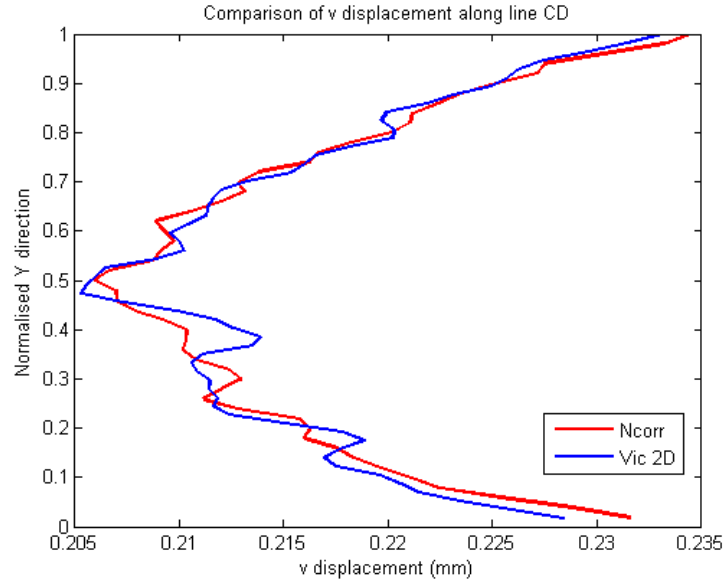


Figure 2.15: Comparison of v displacement along the line CD between Ncorr and Vic 2D estimates

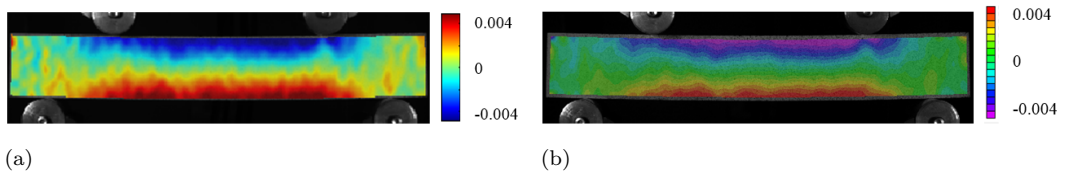


Figure 2.16: ϵ_{xx} contours for an epoxy beam under four point bending using (a) Ncorr (b) Vic 2D

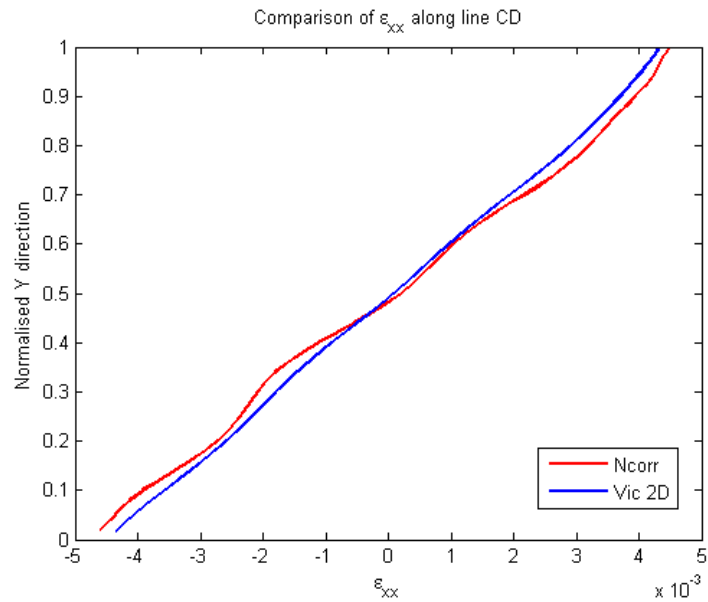


Figure 2.17: Comparison of ϵ_{xx} values obtained by Ncorr and Vic 2D along the line CD

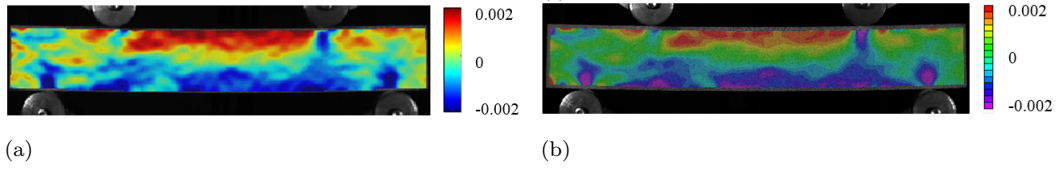


Figure 2.18: ϵ_{yy} contours for an epoxy beam under four point bending using (a) Ncorr (b) Vic 2D

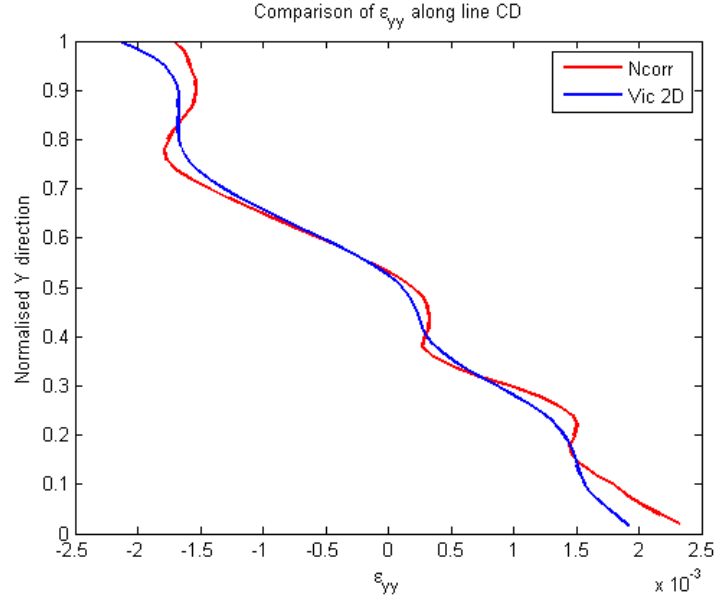


Figure 2.19: Comparison of ϵ_{yy} values obtained by Ncorr and Vic 2D along the line CD

2.5 Smoothing algorithm implementation in Ncorr

Smoothing a given data is to implement a function that can lower the noise and identify the important patterns in the actual data without losing the original trend of it. Various algorithms for smoothing have been implemented throughout the years. Savitzky-Golay filter, Moving Average filter, Median Absolute Deviation are some of the filters that have been used to smooth data. In Savitzky-Golay filter a low degree polynomial is fitted into adjacent subsets and in moving average filter the values in the subsets are averaged and the subsets are shifted after each calculation. In both of these algorithms outliers affect the final result. The algorithms implemented in this study are based on median absolute deviation and mean absolute deviation principle to smooth the displacement data directly obtained from DIC technique. Generally to smooth data, regression analysis is used to establish a relationship between the dependent and the independent variables in order to fit a polynomial curve of degree n [55]. There are many techniques available for doing regression analysis and they can be broadly classified into two categories namely, parametric and non-parametric. Linear regression and ordinary least squares regression are included under parametric methods. In these methods, the data given is used to find parameters of a predefined regression function. The non-parametric methods include methods like loess and lowess, where the form of regression function is not specified in advance but is estimated from a set of functions which are smooth and

continuous involving the given data. Loess is a non-parametric regression method in which a p^{th} -order weighted-least-squares polynomial regression is performed [56]. Small subsets of n points are considered around the point to be smoothed and a polynomial fit is performed. In a local regression method, weights are calculated for each point in the data set so as to determine the closeness of that point to the data set base value as a whole. Thus the points that are lying far away will have less weight and thereby will have only less influence when the curve fitting is done. A linear window or span is specified to select the number of nearest points to be chosen for each iteration. Then a regression weight is assigned to each point in the span using a tri-cube function according to Eq.(4).

$$w_i = \left[1 - \left| \frac{x - x_i}{d(x)} \right|^3 \right]^3 \quad (2.1)$$

where $d(x)$ is the distance to the most distant predictor in the span along the abscissa, x is the predictor value and x_i are the nearest neighbors of x in the span .

After the calculation of weights, a weighted linear least-square regression is implemented over subset of the data. A second degree polynomial is used for loess. The polynomial which is obtained from the weighted linear least-square regression is used to find the regression value at the predictor value of interest. This is repeated for each point in the span. The main disadvantage of the loess is that even the outliers, though it may be small, can have an influence in the curve fitting. In this rloess which is a modified form of loess is implemented. In rloess a robust local regression method is used in which the influence of the outliers can be eliminated. In this method after the loess smoothing is done, the residuals are calculated at every point. Then the median of those values are calculated. Later each of them is assigned a robust weight and outliers are eliminated according to Eqs. 2.2 and 2.3.

$$w_i = \left[1 - \left(\frac{r_i}{6M} \right)^2 \right]^2, |r_i| < 6M, \quad (2.2)$$

$$0, |r_i| \geq 6M \quad (2.3)$$

Where w_i is the weight given to the data point i , r_i is the residual of the i^{th} data point produced by the regression smoothing procedure, and M is the median absolute deviation or mean absolute deviation of the residuals. The data is again smoothed using the robust weights. Thus the final result is obtained by using both local regression and robust weight. In this study the main focus is to smooth the displacement data before strain computation using median absolute deviation and mean absolute deviation algorithms.

2.5.1 Boundary Encoding

The experiment was conducted on a disc under diametrical compression which is a simply connected surface. The ncorr uses a region of interest polygon method to detect the boundary and calculate the displacements. The displacement matrix returned has a zero value outside the boundary. Horizontal smoothing and vertical smoothing is done separately. The boundary for the horizontal smoothing is detected by storing the coordinates of the first non-zero digit from left and right. A similar process is used for the vertical smoothing as well.

2.5.2 Experimental Data Acquisition and Processing

The smoothing is performed on the whole field displacement data estimated for an epoxy disc under diametral compression using the 2D DIC technique. The 2D DIC experimental setup consists of a CCD camera of spatial resolution 2448 x 2048 pixels at a frame rate of 15 fps. The CCD camera is mounted with a Tamron lens of 180 mm focal length. Surface of the epoxy disc is coated with a thin layer of white acrylic paint. Using an airbrush carbon black paint is sprayed in the white surface creating random black and white artificial speckle pattern. The epoxy disc is subjected to a diametral load of 1kN using a computer controlled MTS Landmark servo hydraulic system. Images are collected as the loading progresses and are further post processed using Ncorr software for estimating whole field inplane displacement fields. An additional smoothing module comprising of MAD and mean absolute deviation based algorithm is developed in Ncorr. In each case, smoothing is done in two steps, horizontal smoothing followed by vertical.

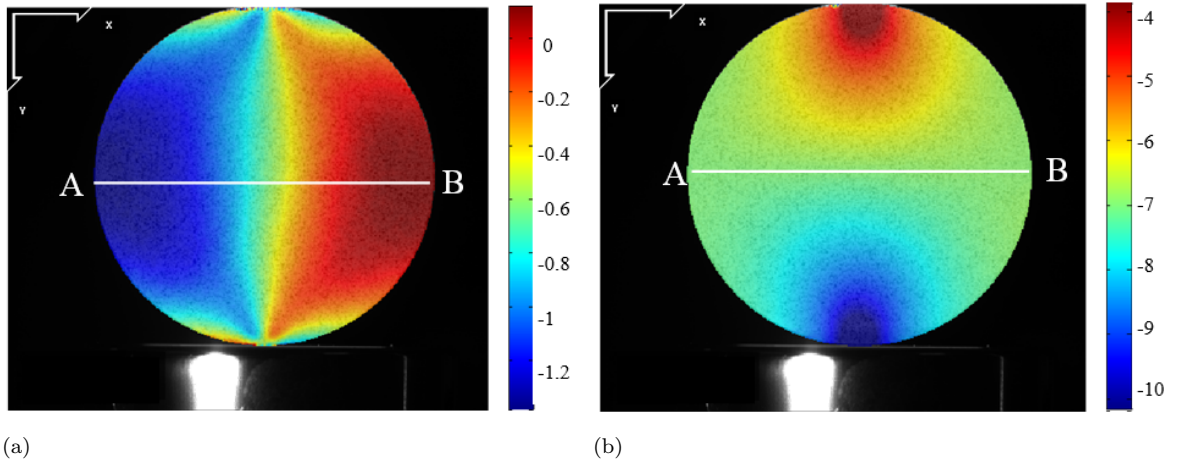
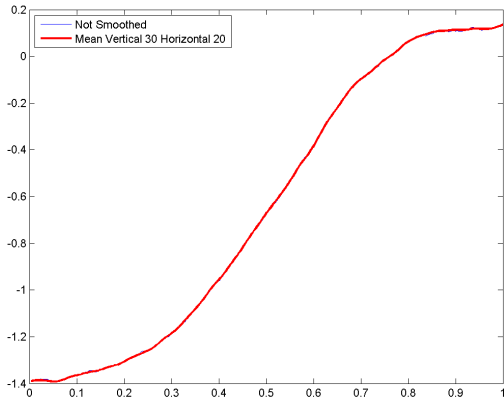


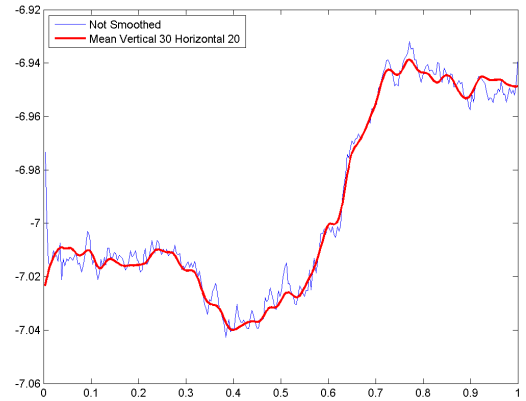
Figure 2.20: Displacement fields obtained using DIC for disc under diametral compression (a) u displacement field (b) v displacement field

2.5.3 Smoothing Using Mean Absolute Deviation

Using the input speckle images, whole field displacement field is computed using Ncorr. A mean absolute deviation based smoothing algorithm is used to smooth the displacement field prior to strain calculation. Fig. 2.21(a) and Fig. 2.21(b) shows the raw and smoothed u and v displacement field using mean absolute deviation for the problem of disc under diametrical compression.

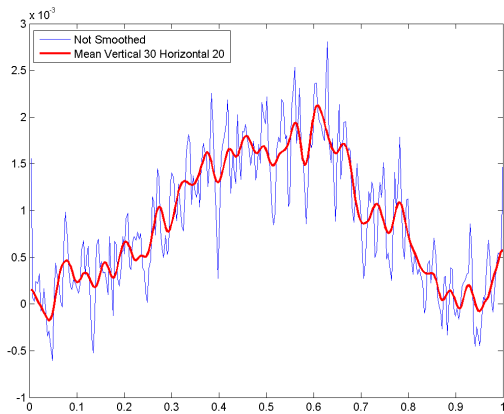


(a)

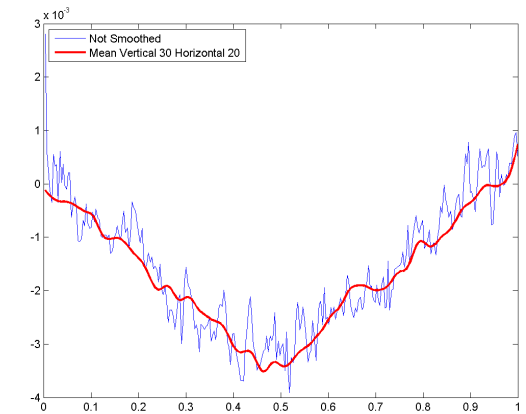


(b)

Figure 2.21: Displacement along line AB smoothed using mean absolute deviation method (a) Comparison of u displacement before and after smoothing (b) comparison of v displacement before and after smoothing



(a)

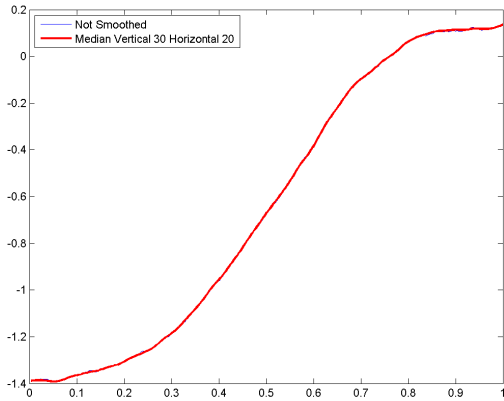


(b)

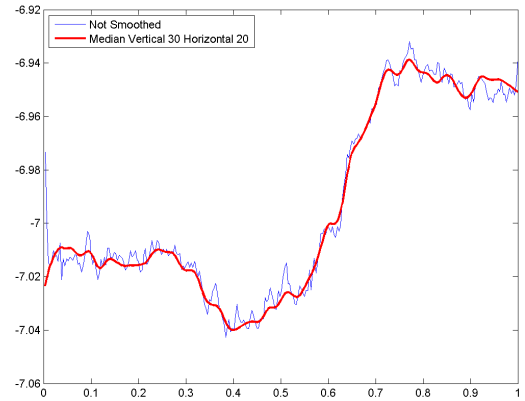
Figure 2.22: Strain along line AB computed from displacement fields smoothed using mean absolute deviation method (a) Comparison of ϵ_{xx} (b) Comparison of ϵ_{yy}

2.5.4 Smoothing Using Median Absolute Deviation

The unsmoothed u and v displacement fields are smoothed using a median absolute deviation based algorithm and are shown in Fig. 2.23(a) and Fig. 2.23(b) respectively

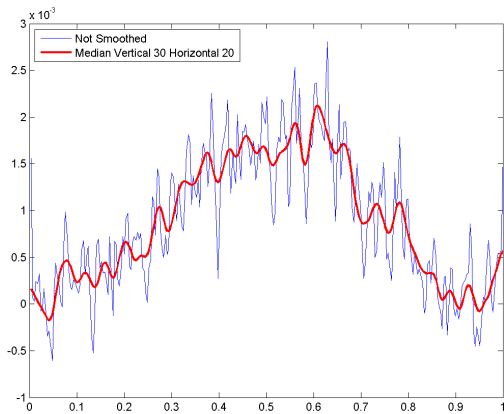


(a)

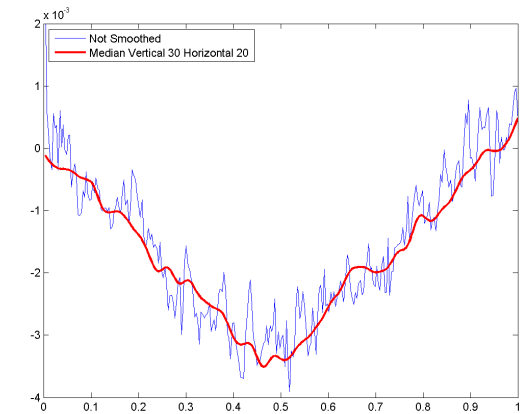


(b)

Figure 2.23: Displacement along line AB smoothed using median absolute deviation method (a) Comparison of u displacement before and after smoothing (b) comparison of v displacement before and after smoothing



(a)



(b)

Figure 2.24: Strain along line AB computed from displacement fields smoothed using median absolute deviation method (a) Comparison of ϵ_{xx} (b) comparison of ϵ_{yy}

2.6 Closure

Two different problems namely, ring under diametral compression and beam under four point bending has been studied. The displacements obtained from Ncorr and Vic 2D for the same set of input images have been compared and are found to be a close match with each other. The strain values being very small in order of magnitude can suffer undulations due to the errors caused from the noise contained in the displacement data during the numerical differentiation. The results obtained are in par with the most widely used Vic 2D software thereby making it a reliable open source alternative for DIC applications. Hence, it is highly recommended for experimental solid mechanics

applications. Further, it forms an integral part of a low cost, accurate DIC system. Since the source code is freely available, users can modify the software based on their requirements.

A whole field smoothing algorithm for the displacement field obtained from DIC has been developed. Both mean and median absolute deviation based algorithms are used to smooth the displacement data prior to strain estimation. Here, problem of disc under diametrical compression is considered. Boundary encoding algorithm is also developed. Both mean and median absolute deviation algorithm tend to give similar results after the smoothing process. An elaborate study needs to be carried out involving the actual influence of span width of the smoothing algorithm on the actual raw experimental data.

Chapter 3

SIF Estimation in SEN and CSC specimen under static loading

3.1 Introduction

Understanding the failure mechanism in structural components subjected to loading is very important for design engineers. It is a well known fact that the presence of flaws such as cracks and sharp notches in the structural components reduce their strength and leads to initiation of fracture and loss of service life. These cracks arise during manufacturing or because of the induced stresses during thermo-mechanical processing such as welding, heat treatment or during service (due to fatigue and/or creep, stress corrosion, thermal loads etc). The presence of the crack results in the redistribution of stresses and strains around the crack-tip. In fracture mechanics, stress intensity factor (SIF) is used to characterize the stress field around the crack tip. The value of crack tip SIF will indicate whether the crack will propagate or not. SIF depends on the far field stress (σ), flaw size (a), component geometry and mode of loading. SIF can be evaluated analytically, numerically and experimentally[57]. Analytical solutions are available for finding SIF for various simple specimen geometries and loading configurations [1]. For complex configurations, SIF need to be extracted either by experiment or by numerical analysis. Numerical methods like finite element method (FEM) requires precise knowledge about the boundary conditions. The experimental methods are particularly well suited for determining SIF for actual geometry and loading conditions. Also, the techniques of experimental stress analysis can be used to verify the solutions obtained from other methods.

In recent years experimental SIF determination involving multi-parameter displacement field equations is gaining popularity among researchers. Traditionally, non-linear over deterministic least square approach has been adopted for extracting crack-tip stress parameters but they have inherent disadvantages especially with respect to convergence. The problem of finding the crack tip stress field parameters and crack tip location can be posed as an optimization problem. The objective function to be minimized is the square of the error between the experimental displacements and curve fitted displacements using multi-parameter displacement field equation. The unknowns to be determined are the crack tip stress field parameters in the multi-parameter displacement field equations along with the crack tip coordinates. It is to be noted that the objective function is not quadratic when we consider the crack tip location as an unknown. Using non-linear least square

algorithm to minimize the objective function one often finds the local minimum leading to a bad curve fit to the experimental data. In this work, we convert the non-linear least square problem into a sequence of linear least square problems. Therefore one can obtain the global minimum of the objective function.

A 2D-DIC technique is employed to get the whole field displacement over the cracked specimens surrounding the crack tip. The cracked specimen is under tensile loading. An open source 2D DIC software Ncorr is used for near crack tip displacement field extraction. From the whole field displacement data, SIFs are estimated by solving multi parameter displacement field equations. The proposed method also predicts the crack tip coordinates with respect to the image coordinate system. Along with the crack tip coordinates, rigid body translations and rotations are also determined. As part of this study, different specimen configurations like single edge notch specimen (SEN) and center slant crack (CSC) made of 2014-T6 aluminium panel are considered.

3.2 Test procedure and Specimen fabrication

The cracked panels are made of Al 2014-T6 aluminium alloy plate with a dimension of 40 x 160 x 3 mm^3 . The material properties of 2014-T6 aluminium alloy is given in Table 3.1 and is taken from the Ref. [58].

Table 3.1: Material properties of 2014-T6 aluminium alloy obtained from the Ref. [58]

Yield Strength	Young's Modulus	Poisson's ratio
433.34 MPa	71.16 GPa	0.332

The straight edge crack of 8 mm was introduced into the specimen using an electro-discharge machining (EDM) wire cut machine. For creating a center crack, initially a 2 mm hole was drilled at the center of the specimen. This hole serves as the passage for the metallic wire of the EDM machine, which was then used to create a 45 degree inclined crack of length 10 mm at the center. Pre-cracking was done by applying fatigue loading in order to generate an initial natural crack with a sharp tip from the notch. During the pre-cracking process, the specimen was monitored closely with a magnifying glass. Liquid dye-penetrant NDT-19 was used to detect any fatigue crack initiation. Using an optical microscope, the lengths of the cracks on both sides of the specimen were measured and the total crack-length was obtained by averaging the two values. The surface of the specimens were then coated with a thin layer of white acrylic paint and sprayed with Carbon black paint using an airbrush to obtain random black-and-white artificial speckle pattern. Fig. 3.1(a) shows the DIC setup and the loading equipment used in the present study. The 2D DIC system comprises of a Grasshopper[®] CCD camera (POINTGREY- GRAS-50S5M-C) of 2448x2048 spatial resolution with a frame rate of 15 fps. A Tamron[®] zoom lens of 185 mm focal length was mounted on the CCD camera and they were connected to a portable computer system with image acquisition card. LED lighting was employed to ensure adequate image contrast. The specimens were loaded using a computer-controlled MTS Landmark[®] servo-hydraulic cyclic testing machine of 100 kN capacity connected to a computer data acquisition system. Load value for every image being captured was recorded using a separate data acquisition system synchronised with the load cell. In order to estimate the SIF at the crack-tip, the camera was aligned with the test specimens such that the

crack faces coincide with horizontal axis of the image co-ordinate system. For SEN specimen, the camera axis was kept horizontal at 0° and for the CSC specimen, the camera axis was inclined by 45° . Figures 3.1(b) and 3.1(c) depict the specimen geometry being considered.

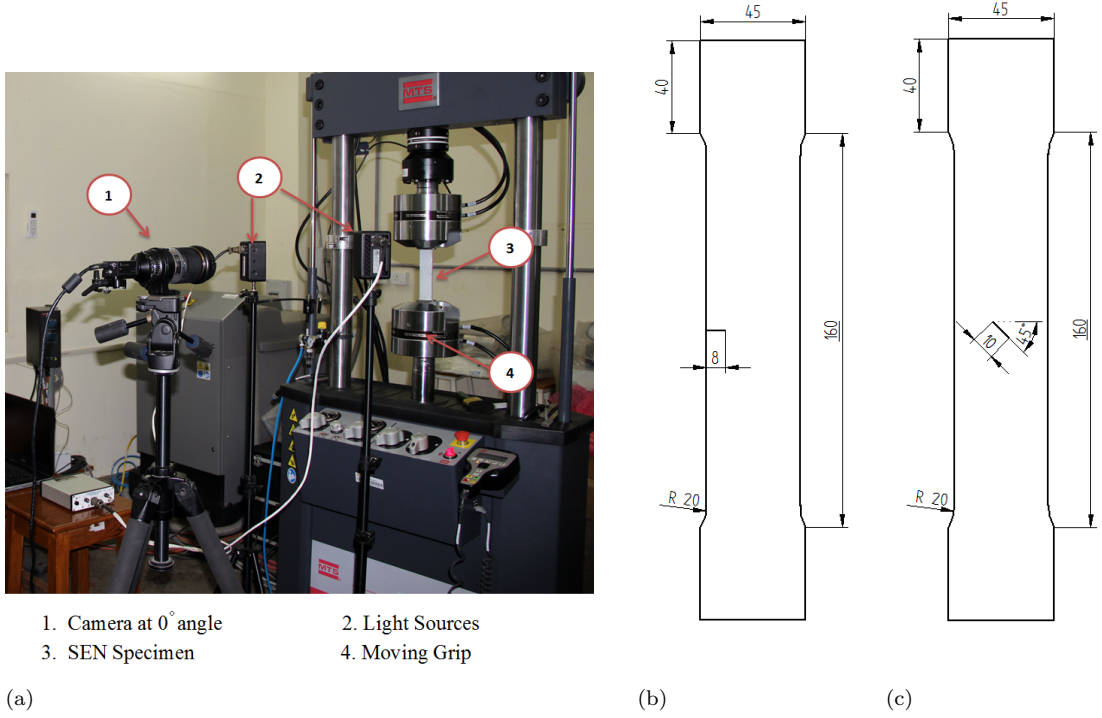


Figure 3.1: Experimental Setup for SIF estimation involving 2D DIC technique along with specimen geometry (a) Experimental setup (b) SEN specimen dimensions in *mm* (c) CSC specimen dimensions in *mm*

3.3 Experimental estimation of SIF

The images obtained from the camera were processed using an open source, MATLAB[®] [53] based 2D DIC software Ncorr [52] developed at Georgia Institute of Technology. This software is used for estimating whole field displacement and strain fields. For SIF estimation, an additional SIF estimation module has been developed by the authors for automated data collection and processing. It involves initial calibration window to map physical real world length scale in terms of pixels. The initial crack tip location can be selected using the graphical user interface (GUI). Data is collected from an annular region surrounding the crack-tip, the inner radius of which is chosen more than half of the specimen thickness to avoid the three-dimensional effects at crack tip and also to avoid non-linear zone in the immediate vicinity of the crack tip. The outer radius of the annular data collection region is limited such that $r/a \leq 1.5$, where a is the crack length and r is the radius [59]. The inner and outer radii, r_i and r_o of the annular zone for data collection can be specified in the graphical user interface (GUI) as shown in the Fig. 3.2(a). An Over-deterministic least square algorithm, proposed by Yoneyama et al. [14, 25] is employed in modified form for the estimation of mixed-mode SIFs from the whole field displacement field. The execution of these algorithm is

explained in detail in the following sub-sections.

3.3.1 Multi-parameter displacement field equations

Atluri and Kobayashi [17] represented the two-dimensional displacement field equations for the general mixed mode crack tip displacement field in a concise form as given below:

$$u_x = \sum_{n=1}^{\infty} \frac{A_{In}}{2G} r^{\frac{n}{2}} \left\{ k \cos \frac{n}{2} \theta - \frac{n}{2} \cos \left(\frac{n}{2} - 2 \right) \theta + \left\{ \frac{n}{2} + (-1)^n \right\} \cos \frac{n}{2} \theta \right\} \\ - \sum_{n=1}^{\infty} \frac{A_{II n}}{2G} r^{\frac{n}{2}} \left\{ k \sin \frac{n}{2} \theta - \frac{n}{2} \sin \left(\frac{n}{2} - 2 \right) \theta + \left\{ \frac{n}{2} - (-1)^n \right\} \sin \frac{n}{2} \theta \right\} \quad (3.1)$$

$$u_y = \sum_{n=1}^{\infty} \frac{A_{In}}{2G} r^{\frac{n}{2}} \left\{ k \sin \frac{n}{2} \theta + \frac{n}{2} \sin \left(\frac{n}{2} - 2 \right) \theta - \left\{ \frac{n}{2} + (-1)^n \right\} \sin \frac{n}{2} \theta \right\} \\ - \sum_{n=1}^{\infty} \frac{A_{II n}}{2G} r^{\frac{n}{2}} \left\{ -k \cos \frac{n}{2} \theta - \frac{n}{2} \cos \left(\frac{n}{2} - 2 \right) \theta + \left\{ \frac{n}{2} - (-1)^n \right\} \cos \frac{n}{2} \theta \right\} \quad (3.2)$$

where u_x and u_y are the displacements along x and y directions respectively, r and θ are the polar coordinates of the data points collected with respect to the crack tip, n is the number of parameters and G is the shear modulus. The parameter $k = (3 - \nu)/(1 + \nu)$ for plane stress condition, here ν is the Poisson's ratio. The other parameters are defined as $A_{I1} = K_I/\sqrt{2\pi}$, $A_{II1} = K_{II}/\sqrt{2\pi}$ and $A_{I2} = -\frac{\sigma_{0x}}{4}$. The parameter σ_{0x} is the T- stress and is used for crack tip characterization.

3.3.2 Solution Procedure

After accounting for rigid body motion, Eq. (3.1) and Eq. (3.2) can be recast in the following form

$$u_x = \sum_{n=1}^{\infty} A_{In} f_I(r, \theta) - \sum_{n=1}^{\infty} A_{II n} f_{II}(r, \theta) + T_x + x(\cos(R) - 1) - y \sin(R) \quad (3.3)$$

$$u_y = \sum_{n=1}^{\infty} A_{In} g_I(r, \theta) - \sum_{n=1}^{\infty} A_{II n} g_{II}(r, \theta) + T_y + y(\cos(R) - 1) + x \sin(R) \quad (3.4)$$

In the above equations (Eq. (3.3) and Eq. (3.4)), T_x and T_y are the rigid body translations in x and y directions and R is the rigid body rotation. The terms f_I , f_{II} , g_I and g_{II} are trigonometric functions of co-ordinates r and θ .

In many cases, it is difficult to find the exact location of the crack-tip due to low spatial resolution of the images being captured. The crack tip location (x_c, y_c) can be treated as unknown parameters along with the coefficients of Eq. (3.3) and Eq. (3.4). The crack tip location is related to r and θ as

follows:

$$r = \sqrt{(x - x_c)^2 + (y - y_c)^2} \quad (3.5)$$

$$\theta = \tan^{-1} \left(\frac{y - y_c}{x - x_c} \right) \quad (3.6)$$

where, x_c and y_c are the locations of the crack tip relative to an arbitrary cartesian co-ordinate frame whose x and y axes are parallel to that of crack tip co-ordinate system.

For practical computational reasons the number of terms in Eq. (3.3) and Eq. (3.4) are truncated to a finite number. For a single point p , the n parameter Eq. (3.3) and Eq. (3.4) can be rewritten in matrix form as

$$\underbrace{\begin{Bmatrix} u_{xp} \\ u_{yp} \end{Bmatrix}}_{\mathbf{u}_p} = \underbrace{\begin{bmatrix} f_{I1}(r_p, \theta_p) & g_{I1}(r_p, \theta_p) \\ f_{I2}(r_p, \theta_p) & g_{I2}(r_p, \theta_p) \\ \vdots & \vdots \\ f_{In}(r_p, \theta_p) & g_{In}(r_p, \theta_p) \\ -f_{II1}(r_p, \theta_p) & -g_{II1}(r_p, \theta_p) \\ -f_{II2}(r_p, \theta_p) & -g_{II2}(r_p, \theta_p) \\ \vdots & \vdots \\ -f_{II n}(r_p, \theta_p) & -g_{II n}(r_p, \theta_p) \\ 1 & 0 \\ 0 & 1 \\ x_p & y_p \\ -y_p & x_p \end{bmatrix}}_{\mathbf{Q}_p}^T \underbrace{\begin{Bmatrix} A_{I1} \\ A_{I2} \\ \vdots \\ A_{In} \\ A_{II1} \\ A_{II2} \\ \vdots \\ A_{II n} \\ T_x \\ T_y \\ \gamma_1 \\ \gamma_2 \end{Bmatrix}}_{\mathbf{a}} \quad (3.7)$$

Here, $\gamma_1 = \cos(R) - 1$ and $\gamma_2 = \sin(R)$. We can write Eq. (3.7) in the following compact form

$$\mathbf{u}_p = \mathbf{Q}_p^T \mathbf{a} \quad (3.8)$$

For a set of m collected data points surrounding crack tip, the assembled set of matrices for n parameter solution can be written as

$$\mathbf{u} = \mathbf{C}(x_c, y_c) \mathbf{a} \quad (3.9)$$

where $\mathbf{u} = [\mathbf{u}_1^T \mathbf{u}_2^T \dots \mathbf{u}_m^T]^T$ and $\mathbf{C} = [\mathbf{Q}_1^T \mathbf{Q}_2^T \dots \mathbf{Q}_m^T]^T$. Here \mathbf{u} is the vector consisting of displacements obtained from the experimental data. \mathbf{C} is a rectangular matrix of the order $2m \times (2n + 4)$ which is dependent on x_c and y_c and \mathbf{a} is the vector consisting of unknown mode I and mode II parameters along with the translation and rotation terms. We will find the values of x_c , y_c and \mathbf{a} by minimizing the following objective function:

$$J(x_c, y_c, \mathbf{a}) = \frac{1}{2} (\mathbf{u} - \mathbf{C}(x_c, y_c) \mathbf{a})^T (\mathbf{u} - \mathbf{C}(x_c, y_c) \mathbf{a}) \quad (3.10)$$

It should be noted that J is not a quadratic function due to its dependency on the unknown crack tip coordinates x_c and y_c . However, for every known x_c and y_c , the objective function becomes quadratic in parameters and the following closed form solution exists for the unknown parameters (\mathbf{a}) at which the objective function (Eq. (3.10)) attains a global minimum and is given by:

$$\mathbf{a} = (\mathbf{C}^T \mathbf{C})^{-1} \mathbf{C}^T \mathbf{u} \quad (3.11)$$

where $(\mathbf{C}^T \mathbf{C})^{-1} \mathbf{C}^T$ is the pseudo inverse of \mathbf{C} .

We select multiple $(x_{ci}, y_{cj}), i = 1, 2, \dots, p, j = 1, 2, \dots, p$ locations around the crack tip as shown in Fig. 3.2(b) and for each of these location we obtain the unknown parameters \mathbf{a}_{ij} using Eq. (3.11). For every (x_{ci}, y_{cj}) , having known \mathbf{a}_i we calculate J_{ij} . Out of all the grid points (see Fig. 3.2(b)) we select the crack tip location $(x_c^*, y_c^*) = (x_{ci}, y_{cj})$ and unknown parameters $\mathbf{a}^* = \mathbf{a}_{ij}$ corresponding to the location (x_{ci}, y_{cj}) at which J_{ij} attains the lowest value. Mathematically our idea to find the optimal parameters and crack tip location can be represented as follows:

$$[\mathbf{a}^{*T} \quad x_c^* \quad y_c^*]^T = \arg \min \min [J_{ij}, i = 1, 2, \dots, p, j = 1, 2, \dots, p] \quad (3.12)$$

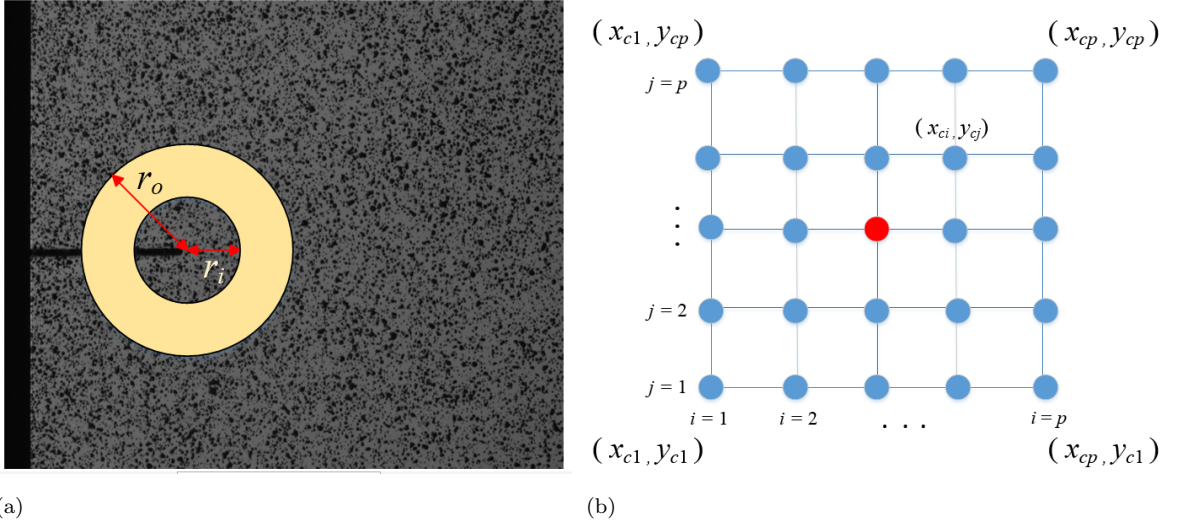


Figure 3.2: Data collection zone and square grid (a) Schematic diagram of the annular region used in data collection for SIF estimation of SEN specimen along with the speckle image (b) Schematic representation of the square grid used for obtaining optimal crack tip location

The procedure for obtaining optimal values of \mathbf{a} and crack tip coordinates (x_c, y_c) presented in this section can be summarized in the algorithmic form as shown below:

Algorithm 1 Algorithm

Minimise the error $J(x_c, y_c, r, n, \mathbf{a})$

for x_c from x_{c1} to x_{cp} **do**

for y_c from y_{c1} to y_{cp} **do**

for r from r_i to r_o **do**

for n from n_s to n_e **do**

$$\mathbf{a} = (\mathbf{C}^T \mathbf{C})^{-1} \mathbf{C}^T \mathbf{u}$$

$$J(x_c, y_c, \mathbf{a}) = \frac{1}{2} (\mathbf{u} - \mathbf{C}(x_c, y_c) \mathbf{a})^T (\mathbf{u} - \mathbf{C}(x_c, y_c) \mathbf{a})$$

end for

end for

end for

end for

$$[\mathbf{a}^{*T} \quad x_c^* \quad y_c^*]^T = \arg \min \min [J_{ij}, i = 1, 2, \dots, p, j = 1, 2, \dots, p]$$

where x_c and y_c are the crack tip coordinates, x_{c1} and x_{cp} are the minimum and maximum x coordinate values of the square grid as shown in Fig. 3.2(b), y_{c1} and y_{cp} are the minimum and maximum y coordinate values of the square grid as shown in Fig. 3.2(b), r_i and r_o are the inner and outer radii of data collection as shown in Fig. 3.2(a), n_s and n_e are the minimum and maximum number of unknown parameters (see Eq. (3.7)).

3.4 Results and Discussions

The displacement data is extracted using an open source 2D DIC software Ncorr which have been found to generate accurate displacement data from input speckle images [60]. The displacement data for SEN and CSC specimens obtained from Ncorr is used as the input for the SIF estimation algorithm to determine the mixed mode SIFs.

3.4.1 Experimental determination of SIF for SEN specimen

Using the automated data collection interface incorporated in the SIF estimation software, both u_x and u_y displacement data are collected within an annular region around the crack tip along with the pixel coordinates obtained for SEN specimen under tensile load (8 kN). An approximate location of the crack tip is selected using the crack tip selection interface. With the selected crack tip as center, a square with 0.2 mm side length and a grid size of 0.02 mm is created. For each of these grid points, the value of \mathbf{a} is computed. The value of \mathbf{a} corresponding to the lowest J value is used to compute K_I . Fig. 3.3 shows the normalized error plot with variation in x and y crack tip coordinates selected from the grid for the case of SEN specimen. The red circle along with an arrow shows the zone of least error.

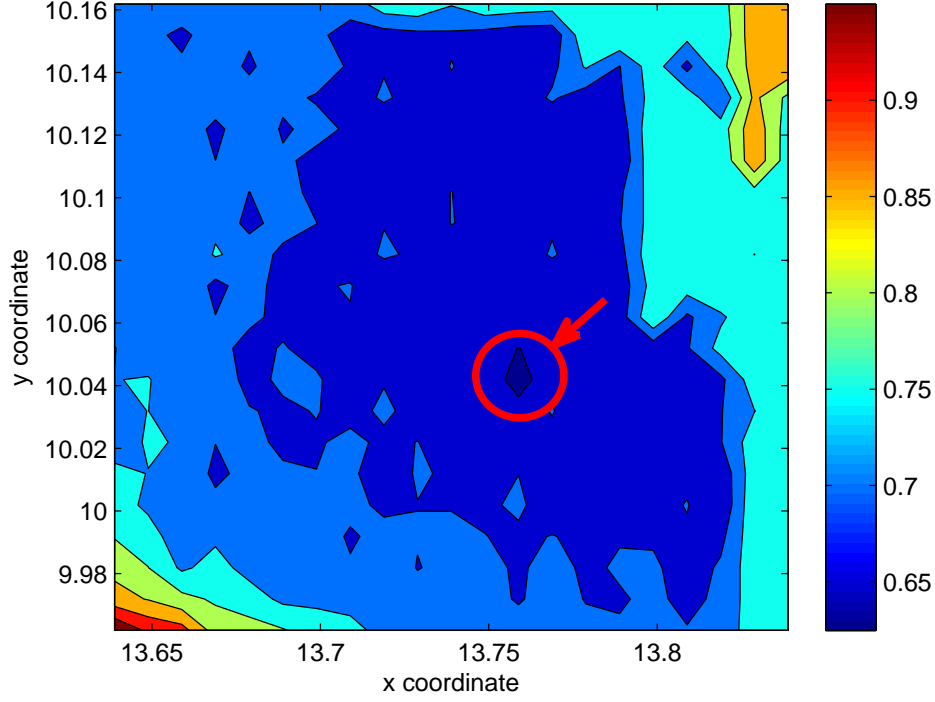


Figure 3.3: Normalized error plot for experimental estimation of SIFs for SEN specimen

The experimentally estimated K_I determined from the relation $A_{I1} = K_I/\sqrt{2\pi}$ is found to be $449.8741 \text{ MPa}\sqrt{\text{mm}}$. The analytical expression of the SIF for SEN specimen [1] is as follows

$$K_I = \sigma\sqrt{\pi a}F(\alpha) \quad (3.13)$$

where σ is the stress due to the applied load and a is the crack length. $F(\alpha)$ can be expanded as

$$F(\alpha) = 1.12 - 0.231\alpha + 10.55\alpha^2 - 21.72\alpha^3 + 30.39\alpha^4$$

where α is crack length to width ratio a/W with a value of 0.2.

Along with the SIF value, the crack tip coordinates, T_x , T_y and R are also estimated. The values of T_x , T_y and R for the 7 parameter solution are found to be -0.03982, 0.1467 and 0.0000457 respectively. It is to be noted that the co-ordinates of the crack-tip are with respect to the image co-ordinate system. The coordinates of the location of the crack tip through manual selection are found to be 13.728 mm and 10.061 mm . After the solution search, the crack tip coordinates corresponding to the least error zone is returned. The x and y coordinates of the predicted crack tip coordinates are found to be 13.768 mm and 10.041 mm . The analytical SIF is calculated using Eq. (3.13) and is found to be $458.0994 \text{ MPa}\sqrt{\text{mm}}$. The experimentally calculated SIF value is found to be close to the analytical value with an error of 1.8%.

The values of different parameters for 2, 4 and 7 parameter solution for SEN specimen are summarized in Table 3.2. As an additional check, the reconstructed and experimental (red markers) displacements fields for 7 parameter solution are superposed on each other in case of SEN specimen and is shown in Fig. 3.4.

Table 3.2: Displacement field parameters for SEN specimen

	2-parameter	4-parameter	7-parameter
K_I (MPa \sqrt{mm})	282.4899	380.8687	449.8741
A_{I1} (MPa(mm) $^{1/2}$)	108.4066	150.8950	175.3587
A_{I2} (MPa)	-13.3757	-22.1636	-29.0510
A_{I3} (MPa(mm) $^{-1/2}$)		7.8054	8.6279
A_{I4} (MPa(mm) $^{-1}$)		-0.5936	0.05096
A_{I5} (MPa(mm) $^{-3/2}$)			-0.6144
A_{I6} (MPa(mm) $^{-2}$)			0.1012
A_{I7} (MPa(mm) $^{-5/2}$)			-0.0148

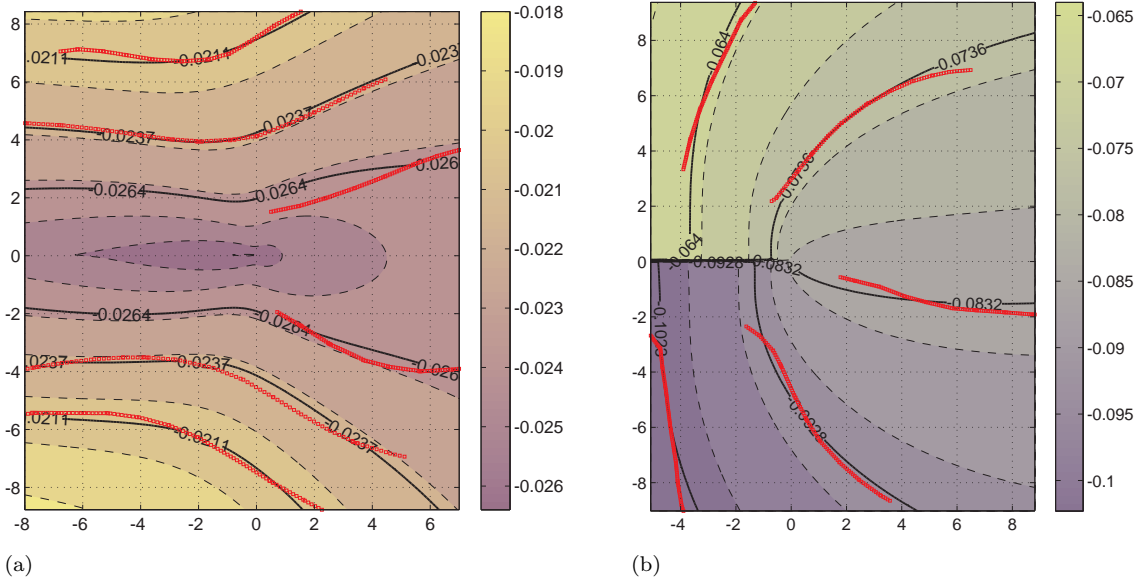


Figure 3.4: Reconstructed and experimental (red markers) displacements fields for 7 parameter solution superposed on each other in case of SEN specimen (a) u_x displacement field (in mm)(b) u_y displacement field (in mm)

3.4.2 Experimental determination of SIF for CSC specimen

The same procedure of data collection used for the SIF estimation in the case of SEN specimen as explained in section 3.4.1 is followed for CSC specimen as well. Fig. 3.5 shows the normalized error plot with variation in x and y crack tip coordinates selected from the grid for CSC specimen at a tensile load of 4 kN. The red circle and arrow shows the zone of least error. The analytical values

of K_I and K_{II} for the CSC specimen are estimated from the expressions taken from Ref. [1]

$$K_I = \sigma\sqrt{\pi a}F_I(\alpha), \quad K_{II} = \sigma\sqrt{\pi a}F_{II}(\alpha) \quad (3.14)$$

The F_I and F_{II} values are found to be 0.5181 and 0.5072 for a 45° center inclined crack respectively [1]. The analytical values of K_I and K_{II} for the given loading condition are found to be $68.4467 \text{ MPa}\sqrt{\text{mm}}$ and $67.0067 \text{ MPa}\sqrt{\text{mm}}$ respectively [1]. The experimentally estimated K_I and K_{II} values are found to be $62.9468 \text{ MPa}\sqrt{\text{mm}}$ and $62.5198 \text{ MPa}\sqrt{\text{mm}}$ respectively. Here too, the seven parameter solution is found accurate as the reconstructed displacement field coincides accurately with the experimental data (See Fig. 3.6). The percentage deviation in experimentally determined K_I and K_{II} values from the analytical values are 8.035% and 6.69% respectively. The values of T_x , T_y and R for the 7 parameter solution is found to be 0.07193, 0.0731 and 0.000568 respectively. The coordinates of the location of the crack tip through manual selection are found to be 12.8314 and 15.7639 (in mm). The x and y coordinates of the predicted location of the crack tip are found to be 12.618 and 15.783 (in mm). The values of different parameters for 2, 4 and 7 parameter solution estimated for the CSC specimen are summarised in Table 3.3.

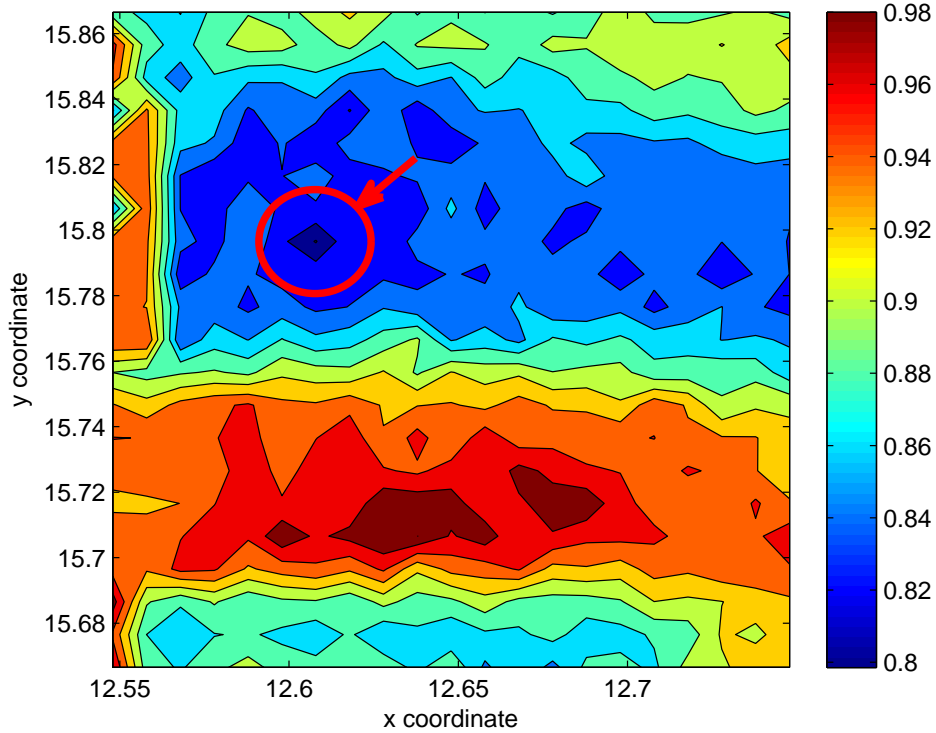


Figure 3.5: Normalized error plot for experimental estimation of SIFs for SEN specimen

Table 3.3: Displacement field parameters for CSC specimen

	2-parameter	4-parameter	7-parameter
K_I (MPa \sqrt{mm})	33.9822	94.5614	62.9468
K_{II} (MPa \sqrt{mm})	78.8870	70.8966	62.5198
A_{I1} (MPa(mm) $^{1/2}$)	13.5569	37.7245	25.1121
A_{I2} (MPa)	0.2298	-6.6442	2.1702
A_{I3} (MPa(mm) $^{-1/2}$)		8.4157	5.9959
A_{I4} (MPa(mm) $^{-1}$)		-0.6307	-0.5789
A_{I5} (MPa(mm) $^{-3/2}$)			0.9902
A_{I6} (MPa(mm) $^{-2}$)			-0.1906
A_{I7} (MPa(mm) $^{-5/2}$)			0.1403
A_{II1} (MPa(mm) $^{1/2}$)	31.4713	28.2836	24.9418
A_{II2} (MPa)	0.0000	0.0000	0.0000
A_{II3} (MPa(mm) $^{-1/2}$)		4.6796	4.3665
A_{II4} (MPa(mm) $^{-1}$)		-0.5292	-1.3957
A_{II5} (MPa(mm) $^{-3/2}$)			0.6901
A_{II6} (MPa(mm) $^{-2}$)			-0.3779
A_{II7} (MPa(mm) $^{-5/2}$)			0.07116

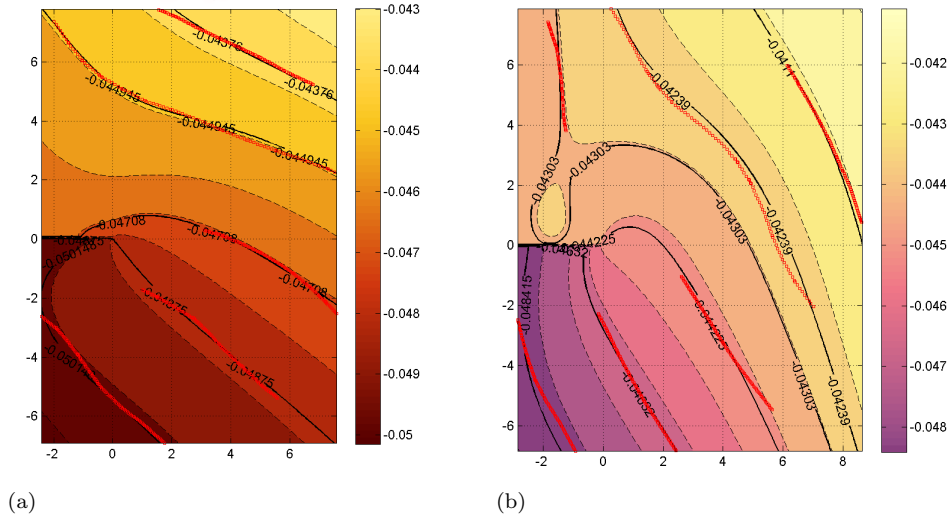
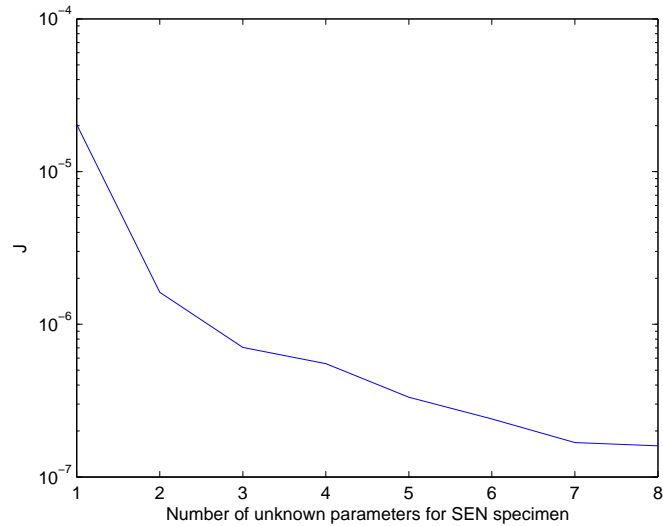


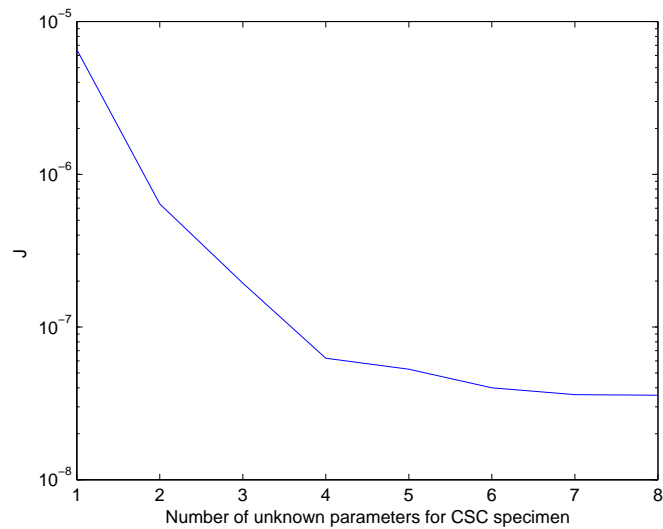
Figure 3.6: Reconstructed and experimental (red markers) displacements fields for 7 parameter solution superposed on each other in case of CSC specimen (a) u_x displacement field (in mm)(b) u_y displacement field (in mm)

The SIF values for SEN and CSC specimens determined above are using 7 parameters in the series solution for u_x and u_y in the multi-parameter displacement field equation (see Eq. (3.1) and

Eq. (3.2)). To select the number of parameters required for the solution process, a convergence study has been done. It has been found that J (see Eq. (3.10)) attains a constant value after iteratively increasing the number of parameters to 7 for both SEN and CSC specimens as shown in Fig. 3.7(a) and Fig. 3.7(b) respectively. Therefore, seven parameters are recommended for SIF estimation.



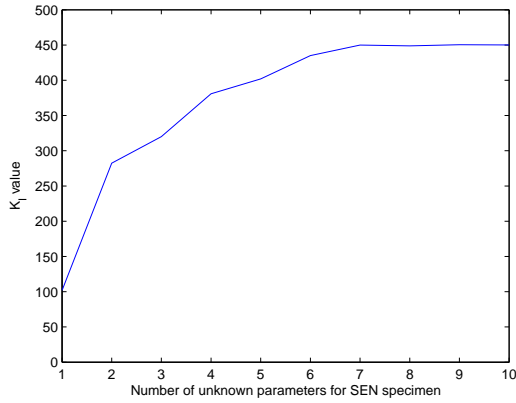
(a)



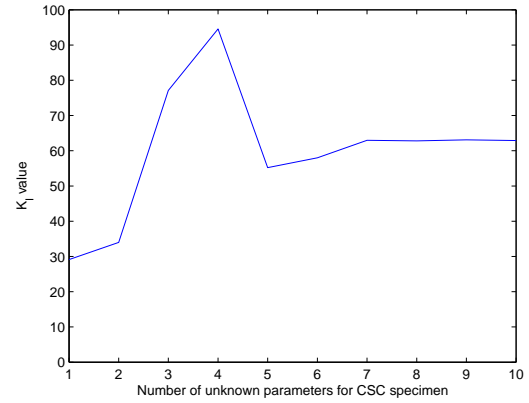
(b)

Figure 3.7: J value with increasing number of parameters (a) J value with increasing number of parameters for SEN specimen (b) J value with increasing number of parameters for CSC specimen

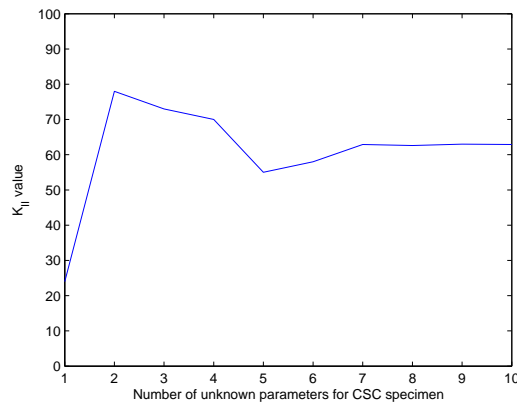
With the increase in number of parameters, the mixed mode SIF values converge. With further increase in parameter values after 7, no significant change in SIF value is observed. This is true for both SEN and CSC specimens as shown in Figs. 3.8(a), 3.8(b) and 3.8(c). Therefore, in general seven parameters are considered for accurate SIF estimation.



(a)



(b)



(c)

Figure 3.8: Variation of mixed mode SIFs for SEN and CSC specimens with increase in n (a) Variation of K_I with increasing number of parameters (n) for SEN specimen (b) Variation of K_I with increasing number of parameters (n) for CSC specimen (c) Variation of K_{II} with increasing number of parameters (n) for CSC specimen

3.5 Closure

In this chapter, an experimental study is carried out to estimate the fracture parameters in cracked aluminium panels. Here, both SEN and CSC specimen configurations are studied. Full field displacement field near the crack tip is estimated using 2D-DIC. An over-deterministic linear least square technique is successfully implemented for SIF measurement involving multi-parameter displacement field equation. This approach is much faster than the conventional iterative scheme existing in the literature [13, 14]. Apart from SIF extraction, a new optimisation based approach is also integrated for extracting crack tip coordinate location. Further, rigid body terms are also determined to make it a complete study. The estimated SIF values for both the specimen configurations are found to be in close match with the analytical estimates, thereby confirming the accuracy of the developed methodology.

Chapter 4

Fatigue crack growth study in a CFRP patch repaired Al2014-T6 panel having an inclined crack involving DIC technique

4.1 Introduction

An aircraft is subjected to severe structural and aerodynamic loads arising from frequent take offs, landings, turbulence and occasional bird strikes. Continuous maintenance at regular intervals are required for an aircraft for its satisfactory performance and safe flight. The metal structural repairs are to be made according to the best possible techniques because improper repair techniques can pose an immediate or potential danger to the structural integrity of the aircraft. Majority of the damage in aircraft arise due to fatigue. Damages due to fatigue is initiated with the formation of fine cracks from high stress zones in the aircraft structure. These cracks if left unattended, can grow at an alarming rate leading to catastrophic failure. To prevent such failures repairs are done to arrest further crack growth. Repair of cracked components in an aircraft using adhesively bonded composite patch can improve the fatigue life and structural integrity of the aircraft. The adhesively bonded repair can reduce the stresses in the cracked regions by effective load transfer through the patch and thereby arresting the crack growth. The fiber composite patches are highly durable under cyclic loading and are characterized by improved directional stiffness, low density and excellent formability.

In the present work, an optimization problem is defined to determine the crack tip stress field parameters and crack tip location. A 2D-DIC technique is employed to get the whole field displacements over the cracked specimens surrounding the crack tip. The objective function to be minimized is the square of the error between the experimental displacements and curve fitted displacements using multi-parameter displacement field equation. We compare SIF values of different specimen configurations like un-repaired cracked aluminium panel and CFRP patch repaired cracked aluminium panel with their FEA estimates from reference [43]. The cracked specimens are subjected

to constant amplitude fatigue loading.

4.2 Geometry and specimen preparation

This section describes the material properties and geometry of un-repaired and single sided patch repaired panel configurations.

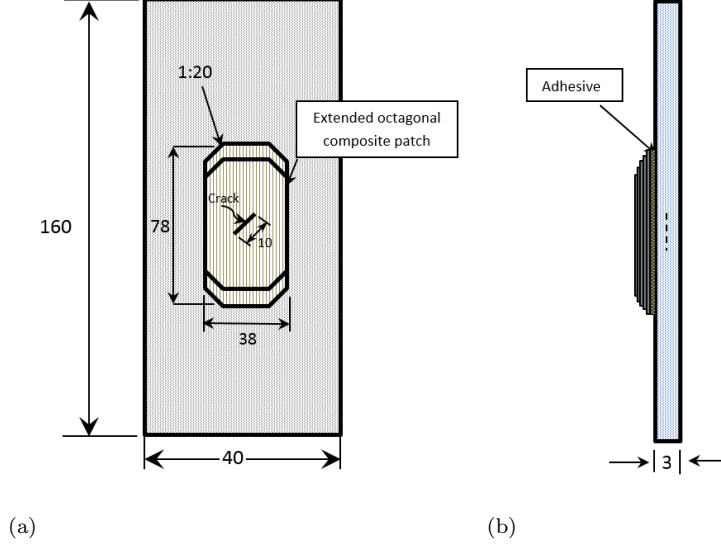


Figure 4.1: Single sided CFRP patch repaired panel (a) Front view showing the adhesively bonded patch over the cracked surface (b) Side view (All dimensions in mm)

The cracked panel is made of aluminium 2014-T6 alloy with dimensions $40 \times 160 \times 3 \text{ mm}^3$ with a 45° inclined crack of length 10 mm at the center. The CFRP patch is bonded using Araldite 2011 adhesive material over one side of the panel to create a single sided patch repaired configuration. The bonded CFRP patch has extended octagonal shape with tapered edges in order to reduce the SIF as shown in Ref. [34]. The size of the CFRP patch is $38 \times 78 \times 2.1 \text{ mm}^3$ obtained using the finite element based optimization technique as explained in Ref. [61]. The CFRP patch is of $[0^\circ]_6$ layup configuration and each lamina is having a thickness of 0.35 mm . The material properties of the Al 2014-T6 panel, CFRP patch laminate and the adhesive (Araldite 2011) are listed in the Table 4.1 and are taken from ref. [61, 62, 63, 64].

Table 4.1: Material properties

Material	E_x (GPa)	$E_y = E_z$ (GPa)	$\nu_{xy} = \nu_{xz}$	ν_{yz}	$G_{xy} = G_{xz}$ (GPa)	G_{yz} (GPa)
Al 2014-T6 [61, 62]	73.1	-	0.33	-	27.48	-
Araldite 2011 [63]	1.148	-	0.4	-	0.41	-
CFRP [64]	81.9	6.15	0.34	0.5	2.77	2.05

The sample preparation is explained in detail in ref. [61]. The CFRP patch is made by hand layup and the cracked aluminium panel is fabricated using wire cut electrical discharge machining (EDM).

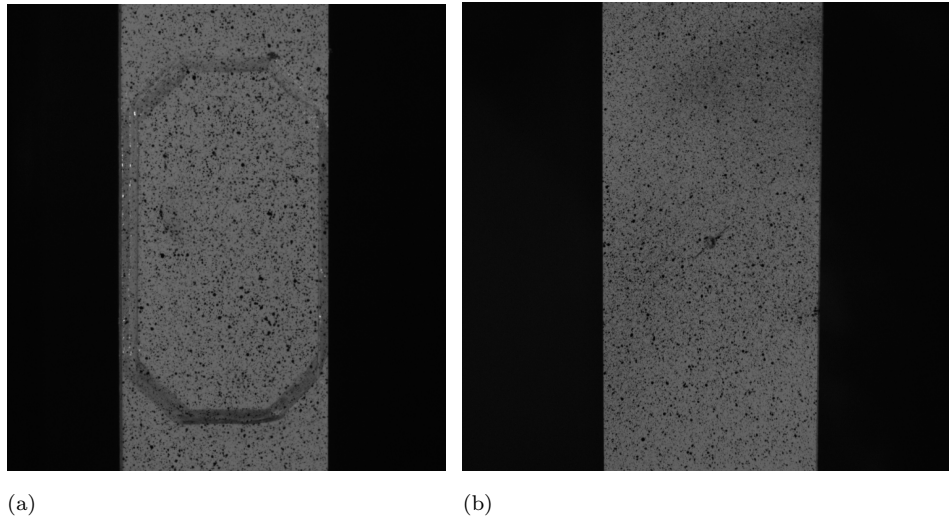


Figure 4.2: Single sided CFRP patch repaired panel with speckle pattern (a) Front view showing the adhesively bonded patch over the cracked surface (b) Rear view with 45 degree inclined crack

4.3 Experimental setup

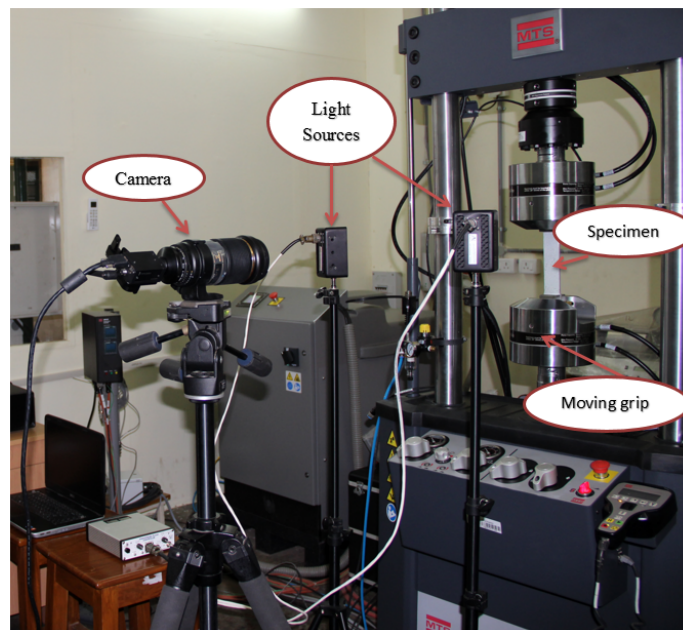


Figure 4.3: Experimental setup

Experiments are performed in MTS[®] servo hydraulic cyclic loading machine of 100 kN capacity connected to a computer data acquisition system. Specimens are subjected to constant amplitude tension–tension fatigue load (0.7 to 14.16 kN) at a frequency of 10 Hz. The crack length and displacement fields around the crack tip are obtained using 2D DIC technique. The 2D DIC system comprises of a Grasshopper[®] CCD camera (POINTGREY- GRAS-50S5M-C) with a spatial resolu-

tion 2448 x 2048 pixels and a frame rate of 15 fps. A Tamron[®] zoom lens of 185 mm focal length is mounted on the CCD camera which is connected to a laptop computer with image acquisition hardware. LED lighting is employed to obtain the required image contrast. Load value for every image being captured is recorded using a separate data acquisition system synchronized with the load cell. The u_x and u_y displacements are extracted from the captured images using open source 2D DIC software Ncorr [65].

4.4 Experimental SIF evaluation

For SIF estimation, authors have developed an additional SIF Estimation module which has automated data collection and processing capabilities. It includes an initial calibration window to map physical real world length scale in terms of pixel values. A graphical user interface (GUI) facilitates the selection of initial crack tip location. The displacement data is collected along an annular region surrounding the crack-tip. The inner radius of the annular ring is chosen to be more than half of the specimen thickness to avoid the three-dimensional effects at crack tip as well as to avoid non-linear zone in the immediate vicinity of the crack tip. This criterion is applicable for thin plates [59]. The outer radius of the annular region is chosen such that $r/a \leq 1.5$, where a is the crack length and r is the radius. The inner and outer radii for data collection, r_i and r_o can be specified in the graphical user interface (GUI) as shown in the Fig. 4.5(a). The SIF estimation module uses an over-deterministic linear least square algorithm for the estimation of mixed-mode SIFs based on whole field displacement field. The algorithm and its implementation is explained in detail in the following sub-sections.

4.4.1 Multi-parameter displacement field equations

Atluri and Kobayashi [66, 67] formulated the two-dimensional displacement field equations for the general mixed mode crack tip displacement field as shown below

$$u_x = \sum_{n=1}^{\infty} \frac{A_{In}}{2G} r^{\frac{n}{2}} \left\{ k \cos \frac{n}{2} \theta - \frac{n}{2} \cos \left(\frac{n}{2} - 2 \right) \theta + \left\{ \frac{n}{2} + (-1)^n \right\} \cos \frac{n}{2} \theta \right\} \\ - \sum_{n=1}^{\infty} \frac{A_{II n}}{2G} r^{\frac{n}{2}} \left\{ k \sin \frac{n}{2} \theta - \frac{n}{2} \sin \left(\frac{n}{2} - 2 \right) \theta + \left\{ \frac{n}{2} - (-1)^n \right\} \sin \frac{n}{2} \theta \right\} \quad (4.1)$$

$$u_y = \sum_{n=1}^{\infty} \frac{A_{In}}{2G} r^{\frac{n}{2}} \left\{ k \sin \frac{n}{2} \theta + \frac{n}{2} \sin \left(\frac{n}{2} - 2 \right) \theta - \left\{ \frac{n}{2} + (-1)^n \right\} \sin \frac{n}{2} \theta \right\} \\ - \sum_{n=1}^{\infty} \frac{A_{II n}}{2G} r^{\frac{n}{2}} \left\{ -k \cos \frac{n}{2} \theta - \frac{n}{2} \cos \left(\frac{n}{2} - 2 \right) \theta + \left\{ \frac{n}{2} - (-1)^n \right\} \cos \frac{n}{2} \theta \right\} \quad (4.2)$$

where r and θ are the polar coordinates of the data point collected with respect to the crack tip, u_x and u_y are the displacements along x and y directions respectively, n is the number of parameters and G is the shear modulus. The parameter $k = (3 - \nu)/(1 + \nu)$ is for plane stress condition, where ν is the Poisson's ratio. The other parameters are defined as $A_{I1} = K_I/\sqrt{2\pi}$, $A_{II1} = K_{II}/\sqrt{2\pi}$ and $A_{I2} = -\frac{\sigma_{0x}}{4}$. The parameter σ_{0x} is the T- stress and is also used for crack tip characterization.

4.4.2 Solution Procedure

The above multi-parameter equations can be expressed in the following form after accounting for the rigid body motion

$$u_x = \sum_{n=1}^{\infty} A_{In} f_I(r, \theta) - \sum_{n=1}^{\infty} A_{II n} f_{II}(r, \theta) + T_x + x(\cos(R) - 1) - y \sin(R) \quad (4.3)$$

$$u_y = \sum_{n=1}^{\infty} A_{In} g_I(r, \theta) - \sum_{n=1}^{\infty} A_{II n} g_{II}(r, \theta) + T_y + y(\cos(R) - 1) + x \sin(R) \quad (4.4)$$

Here, T_x and T_y represent the rigid body translations along x and y directions. R is the rigid body rotation. The terms f_I , f_{II} , g_I and g_{II} are trigonometric functions in r and θ .

The spatial resolution of the images captured during the loading cycle plays an important role in identifying the accurate location of the crack tip. In many cases, the low spatial resolution of the images being captured makes it difficult to find the exact location of the crack-tip. The crack tip x and y coordinates (x_c, y_c) can be treated as unknown parameters along with the coefficients of Eq. (4.3) and Eq. (4.4). The coordinates r and θ can be expressed in terms of crack tip location as follows:

$$r = \sqrt{(x - x_c)^2 + (y - y_c)^2} \quad (4.5)$$

$$\theta = \tan^{-1} \left(\frac{y - y_c}{x - x_c} \right) \quad (4.6)$$

where, x_c and y_c are the locations of the crack tip relative to an arbitrary cartesian co-ordinate frame whose x and y axes are parallel to that of crack tip co-ordinate system.

The number of terms in Eq. (4.3) and Eq. (4.4) are truncated to a finite number for practical computational reasons. For a single point p , the n parameter Eq. (4.3) and Eq. (4.4) can be rewritten in matrix form as follows

$$\underbrace{\begin{Bmatrix} u_{xp} \\ u_{yp} \end{Bmatrix}}_{\mathbf{u}_p} = \underbrace{\begin{bmatrix} f_{I1}(r_p, \theta_p) & g_{I1}(r_p, \theta_p) \\ f_{I2}(r_p, \theta_p) & g_{I2}(r_p, \theta_p) \\ \vdots & \vdots \\ f_{In}(r_p, \theta_p) & g_{In}(r_p, \theta_p) \\ -f_{II1}(r_p, \theta_p) & -g_{II1}(r_p, \theta_p) \\ -f_{II2}(r_p, \theta_p) & -g_{II2}(r_p, \theta_p) \\ \vdots & \vdots \\ -f_{II n}(r_p, \theta_p) & -g_{II n}(r_p, \theta_p) \\ 1 & 0 \\ 0 & 1 \\ x_p & y_p \\ -y_p & x_p \end{bmatrix}}_{\mathbf{Q}_p}^T \underbrace{\begin{Bmatrix} A_{I1} \\ A_{I2} \\ \vdots \\ A_{In} \\ A_{II1} \\ A_{II2} \\ \vdots \\ A_{II n} \\ T_x \\ T_y \\ \gamma_1 \\ \gamma_2 \end{Bmatrix}}_{\mathbf{a}} \quad (4.7)$$

Here, $\gamma_1 = \cos(R) - 1$ and $\gamma_2 = \sin(R)$. We can represent Eq. (4.7) in a compact form as shown below

$$\mathbf{u}_p = \mathbf{Q}_p^T \mathbf{a} \quad (4.8)$$

For a set of m collected data points around the crack tip, the assembled set of matrices for n parameter solution can be written as

$$\mathbf{u} = \mathbf{C}(x_c, y_c) \mathbf{a} \quad (4.9)$$

where $\mathbf{u} = [\mathbf{u}_1^T \ \mathbf{u}_2^T \ \dots \ \mathbf{u}_m^T]^T$ and $\mathbf{C} = [\mathbf{Q}_1^T \ \mathbf{Q}_2^T \ \dots \ \mathbf{Q}_m^T]^T$. Here, \mathbf{u} is the vector consisting of displacements obtained from the DIC technique. \mathbf{C} is a rectangular matrix of the order $2m \times (2n+4)$ which is dependent on x_c and y_c and \mathbf{a} is the vector consisting of unknown mode I and mode II parameters along with the translation and rotation terms. The values of x_c , y_c and \mathbf{a} can be obtained by minimizing the following objective function:

$$J(x_c, y_c, \mathbf{a}) = \frac{1}{2}(\mathbf{u} - \mathbf{C}(x_c, y_c) \mathbf{a})^T (\mathbf{u} - \mathbf{C}(x_c, y_c) \mathbf{a}) \quad (4.10)$$

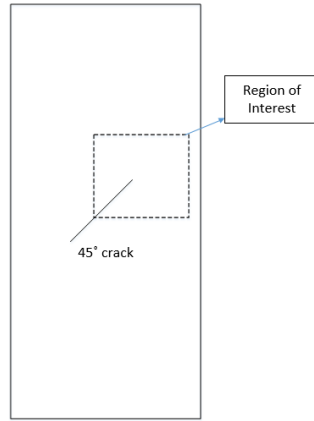
J is dependent on the unknown crack tip coordinates x_c and y_c and hence it is not a quadratic function. However, for every known x_c and y_c , the objective function becomes quadratic in parameters and the following closed form solution exists for the unknown parameters (\mathbf{a}) at which the objective function (Eq. (4.10)) attains a global minimum and is given by:

$$\mathbf{a} = (\mathbf{C}^T \mathbf{C})^{-1} \mathbf{C}^T \mathbf{u} \quad (4.11)$$

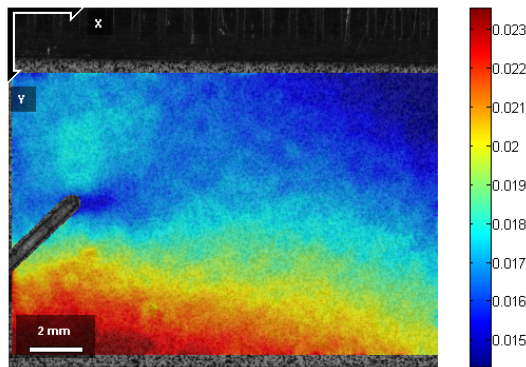
where $(\mathbf{C}^T \mathbf{C})^{-1} \mathbf{C}^T$ is the pseudo inverse of \mathbf{C} .

The region of interest for displacement estimation using DIC for the unrepaired panel is as shown in the Fig. 4.4(a). We select multiple (x_{ci}, y_{cj}) , $i = 1, 2, \dots, p$, $j = 1, 2, \dots, p$ locations around the crack tip as shown in Fig. 4.5(b) and for each of these location we obtain the unknown parameters \mathbf{a}_{ij} using Eq. (4.11). For every (x_{ci}, y_{cj}) , having known \mathbf{a}_i we calculate J_{ij} . Out of all the grid points (see Fig. 4.5(b)) we select the crack tip location $(x_c^*, y_c^*) = (x_{ci}, y_{cj})$ and unknown parameters $\mathbf{a}^* = \mathbf{a}_{ij}$ corresponding to the location (x_{ci}, y_{cj}) at which J_{ij} attains the lowest value. Mathematically our idea to find the optimal parameters and crack tip location can be represented as follows:

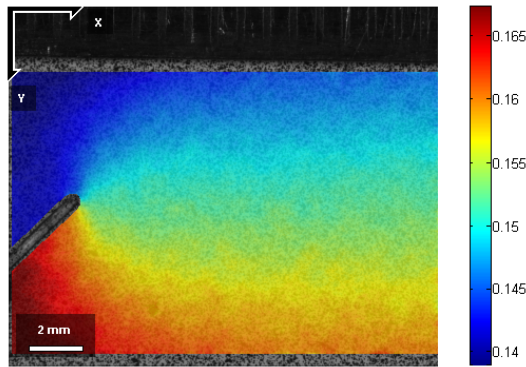
$$[\mathbf{a}^{*T} \ x_c^* \ y_c^*]^T = \arg \min \min [J_{ij}, i = 1, 2, \dots, p, j = 1, 2, \dots, p] \quad (4.12)$$



(a)



(b)



(c)

Figure 4.4: Region of interest chosen for SIF estimation (a) Graphical representation of the considered area (b) u displacement field corresponding to chosen ROI (c) v displacement field corresponding to chosen ROI (All dimensions in mm)

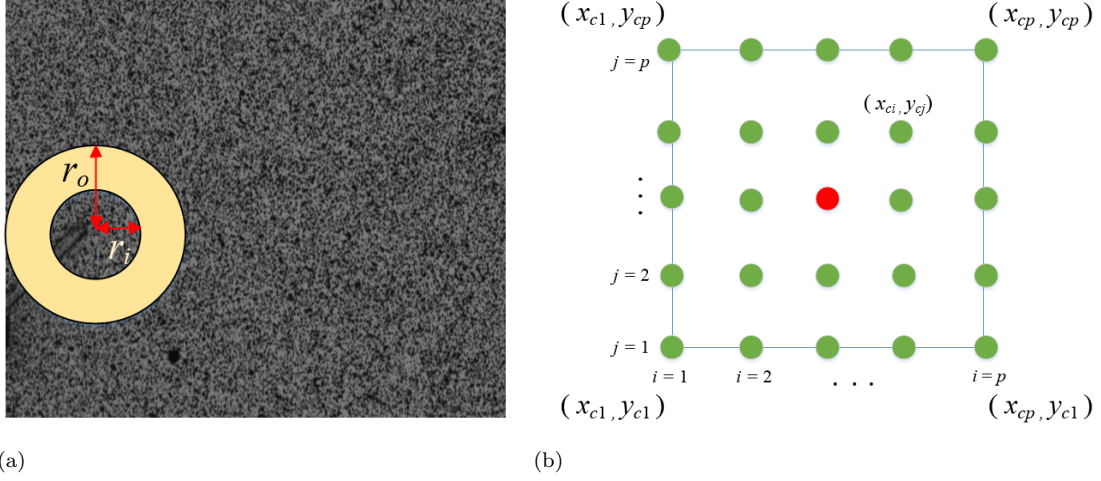


Figure 4.5: Data collection zone for SIF measurement (a) Region of interest chosen for SIF estimation (b) Schematic representation of the square grid used for obtaining optimal crack tip location

The procedure for obtaining optimal values of \mathbf{a} and crack tip coordinates (x_c, y_c) presented in this section can be summarized in the algorithmic form as shown below:

Algorithm 2 Algorithm

Minimise the error $J(x_c, y_c, r, n, \mathbf{a})$

for x_c from x_{c1} to x_{cp} **do**

for y_c from y_{c1} to y_{cp} **do**

for r from r_i to r_o **do**

for n from n_s to n_e **do**

$$\mathbf{a} = (\mathbf{C}^T \mathbf{C})^{-1} \mathbf{C}^T \mathbf{u}$$

$$J(x_c, y_c, \mathbf{a}) = \frac{1}{2} (\mathbf{u} - \mathbf{C}(x_c, y_c) \mathbf{a})^T (\mathbf{u} - \mathbf{C}(x_c, y_c) \mathbf{a})$$

end for

end for

end for

end for

$$[\mathbf{a}^{*T} \quad x_c^* \quad y_c^*]^T = \arg \min \min [J_{ij}, i = 1, 2, \dots, p, j = 1, 2, \dots, p]$$

where x_c and y_c are the crack tip coordinates, x_{c1} and x_{cp} are the minimum and maximum x coordinate values of the square grid as shown in Fig. 4.5(b), y_{c1} and y_{cp} are the minimum and maximum y coordinate values of the square grid as shown in Fig. 4.5(b), r_i and r_o are the inner and outer radii of data collection as shown in Fig. 4.5(a), n_s and n_e are the minimum and maximum number of unknown parameters (see Eq. (4.7)).

4.5 Finite Element Modeling

The finite element model of the cracked panel is created in ANSYS software. Initially, the panel is modeled without the crack tip elements. The 3D crack elements for the crack propagation study is generated by implementing a macro in Zencrack software which can be directly linked to ANSYS. Authors have followed the modeling techniques used in Ref [43] to create the finite element model of the cracked panel. Eight noded solid 185 element is used to mesh the panel with three elements along the thickness direction. A constant amplitude cyclic load of 14.16 kN is applied with a stress ratio (R) of 0.05 to simulate the fatigue crack growth. Zencrack is equipped with adaptive re-meshing at every crack front advancement to simulate fatigue crack growth.

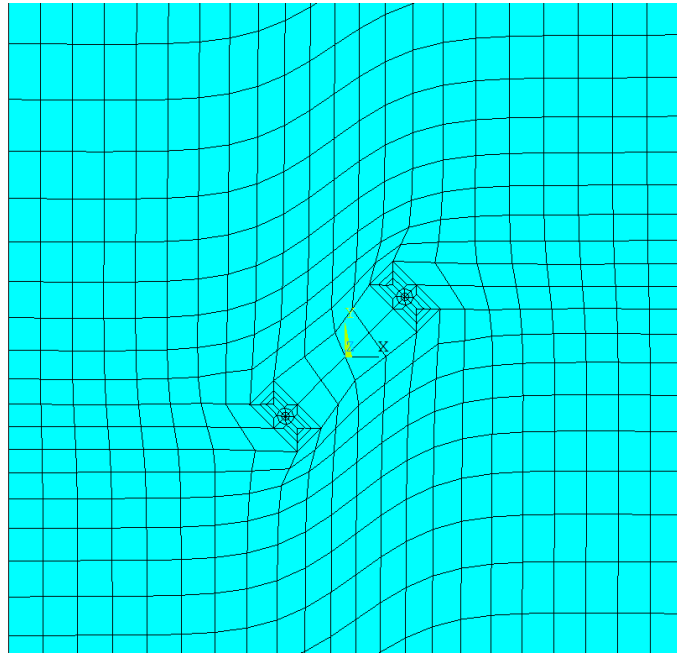


Figure 4.6: FEA mesh with crack blocks

Figure 4.7 shows the v displacement contours obtained from DIC and FEA for unrepaired panel for 5500, 6800 and 8000 fatigue cycles.

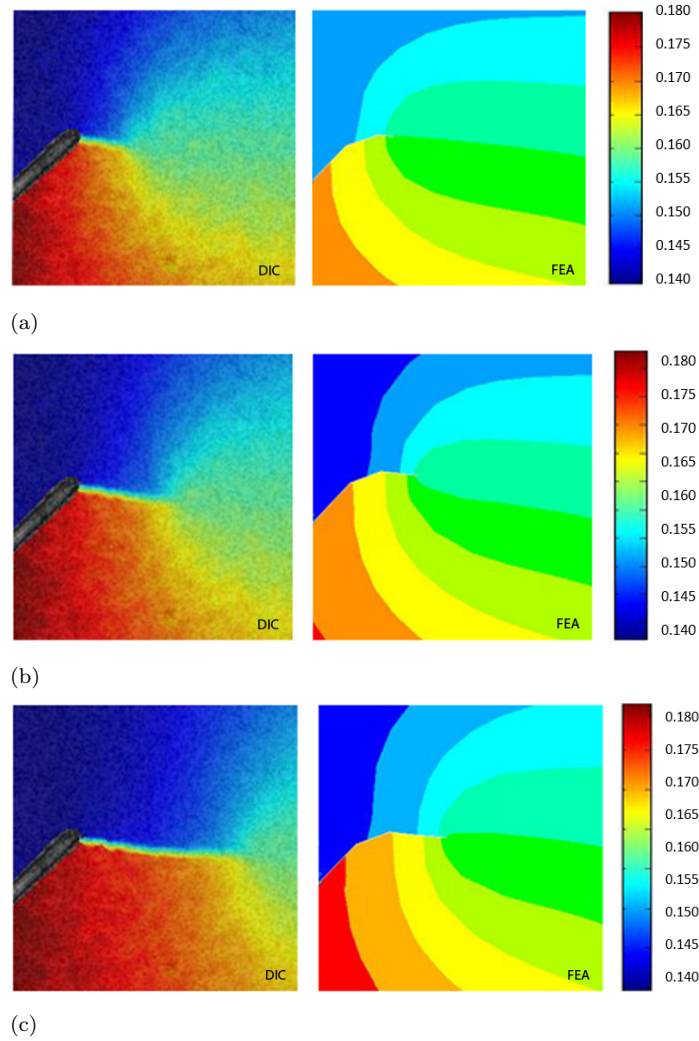
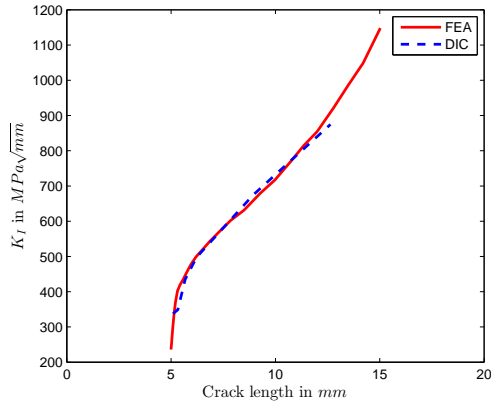


Figure 4.7: v displacement contours from DIC and FEA for unrepaired panel (a) at 5500 cycles (b) at 6800 cycles (c) at 8000 cycles (All measurements in mm)

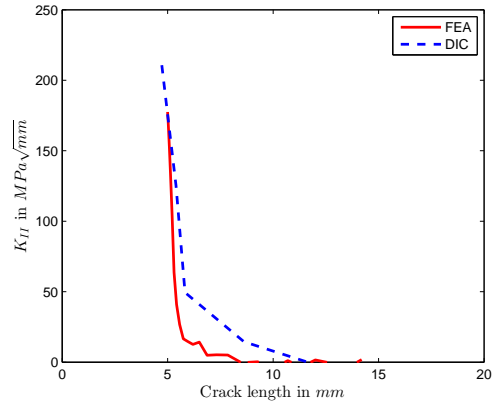
4.6 Results and Discussions

4.6.1 Unrepaired Panel

Figures 4.8(a) and 4.8(b) shows the variation in K_I and K_{II} values with increasing crack length obtained for an un-repaired cracked aluminium panel. The red lines show the data obtained using FEA taken from Ref. [43]. The blue dotted lines shows the variation in SIF with respect to crack length for the data obtained using DIC technique. There is good coherence with FEA and DIC prediction. But DIC prediction is not possible at higher crack length, since the fracture process is very fast due to which not many images have been acquired.



(a)

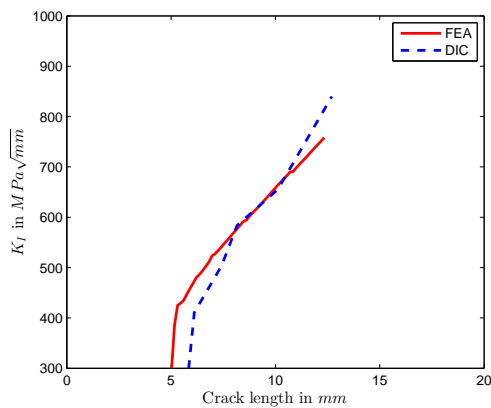


(b)

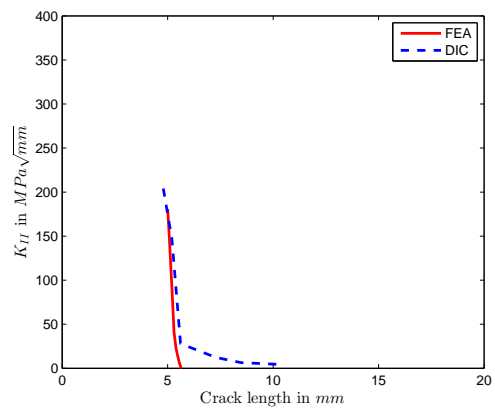
Figure 4.8: Variation of K_I and K_{II} with crack growth for an unrepaired aluminium panel under constant amplitude fatigue load (a) Variation of K_I (b) Variation of K_{II}

4.6.2 Single Sided Repaired Panel

For estimating the SIFs at the crack tip in case of single side repaired specimen, the displacement field obtained over the unpatched surface is considered. Figures 4.9(a) and 4.9(b) shows the variation in K_I and K_{II} values with crack growth for single sided patch repaired aluminium panel. The red lines show the data obtained using FEA taken from Ref. [43]. The blue dotted lines shows the variation in SIF with respect to crack length for the data obtained using DIC technique. There is good coherence between DIC and FEA predictions. Mostly, DIC technique is able to predict the trend as given by FEA results.



(a)



(b)

Figure 4.9: Variation of K_I and K_{II} with increase in crack length for CFRP patch repaired aluminium panel (a) Variation of K_I with increasing crack length in mm (b) Variation of K_{II} with increasing crack length in mm

4.7 Closure

In the present work, an experimental study is carried out to estimate the mixed mode SIFs in un-repaired and CFRP patch repaired cracked aluminium panels under constant amplitude fatigue load. Various images surrounding crack tip are acquired during fatigue cycle until failure and respective SIF's are determined respectively. The computed SIF values are compared with FEA estimates and are found to be in good agreement with each other. Displacement field information surrounding the crack tip is used for SIF estimation. The crack tip displacement field is obtained using 2D DIC technique. A multi parameter displacement field equation is solved in an over deterministic linear least square approach.

Chapter 5

Conclusions and Recommendations

In the present work, a new algorithm is proposed for the estimation of mixed-mode SIFs by solving multi-parameter displacement field equations using the displacement field obtained from digital image correlation technique. Along with the SIFs, the algorithm facilitates the extraction of crack tip location, rigid body translation and rotation components. The required displacement data surrounding the crack tip has been obtained using 2D-DIC technique. An open source 2D DIC software Ncorr is used for displacement extraction from the input speckle images. To establish the credibility of Ncorr, two different problems namely, ring under diametral compression and beam under four point bending has been considered. The results obtained from Ncorr is compared with its commercial counterpart Vic 2D software. The displacements obtained from Ncorr and Vic 2D for the same set of input images have been compared for both the problems. The results obtained are in par with the most widely used Vic 2D software thereby making it a reliable and accurate open source alternative for DIC applications. Hence, it is highly recommended for solid mechanics applications. Further, it forms an integral part of a low cost, accurate DIC system. Since the source code is freely available, users can modify the software based on their requirements. In addition to the validation of Ncorr, a whole field smoothing algorithm for the displacement field obtained from DIC has been developed. Both mean and median absolute deviation based algorithms are used to smooth the displacement data prior to strain estimation. Here, the problem of disc under diametrical compression is considered. Both mean and median absolute deviation algorithm tend to give similar results after the smoothing process. In future, an elaborate study needs to be carried out involving the actual influence of span width of the smoothing algorithm on the actual raw experimental data from DIC technique. An additional SIF estimation module based on the new algorithm for SIF estimation has been developed for the estimation of mixed mode SIFs in case of static and constant amplitude fatigue loading cases.

For the static loading case, two specimen configurations namely single edge notch and center slant crack specimens are studied. An improved over deterministic least square technique is successfully implemented for SIF measurement involving multi-parameter displacement field equation. This approach is much faster than the conventional iterative scheme existing in the literature. Additionally, an optimisation based approach is also integrated to determine the exact crack tip coordinate location. Rigid body terms are also extracted along with the crack tip coordinates. The estimated SIF values for both the specimen configurations are found to be in close match with the analytical

estimates, thereby confirming the accuracy of the developed methodology. For the fatigue loading case un-repaired and CFRP patch repaired cracked Al 2014-T6 specimens are considered. The mixed mode SIFs for increasing number of load cycles are computed. The computed values are compared with FEA estimates from a previous study. The results are found to be in coherence with each other.

In actual practice, the aircraft components are subjected to variable amplitude spectrum cyclic loading. An extension of the developed algorithm for SIF estimation for variable amplitude study would involve many challenges such as synchronization, accurate estimation of crack tip coordinate etc.

References

- [1] Y. Murakami. Stress Intensity Factors Handbook. Pergamon Pr, 1987.
- [2] W. Peters and W. Ranson. Digital imaging techniques in experimental stress analysis. *Optical Engineering* 21, (1982) 213,427–213,427.
- [3] M. Sutton, W. Wolters, W. Peters, W. Ranson, and S. McNeill. Determination of displacements using an improved digital correlation method. *Image and vision computing* 1, (1983) 133–139.
- [4] B. Pan, K. Qian, H. Xie, and A. Asundi. Two-dimensional digital image correlation for in-plane displacement and strain measurement: a review. *Measurement science and technology* 20, (2009) 062,001.
- [5] B. Pan, K. Li, and W. Tong. Fast, robust and accurate digital image correlation calculation without redundant computations. *Experimental Mechanics* 53, (2013) 1277–1289.
- [6] H. Bruck, S. McNeill, M. A. Sutton, and W. Peters Iii. Digital image correlation using Newton-Raphson method of partial differential correction. *Experimental Mechanics* 29, (1989) 261–267.
- [7] M. Sutton, J. Turner, Y. Chao, H. Bruck, and T. Chae. Experimental investigations of three-dimensional effects near a crack tip using computer vision. *International journal of fracture* 53, (1992) 201–228.
- [8] T. Dudderar and H. Gorman. The determination of mode I stress-intensity factors by holographic interferometry. *Experimental Mechanics* 13, (1973) 145–149.
- [9] A. Moore and J. Tyrer. Phase-stepped ESPI and moiré interferometry for measuring stress-intensity factor and J integral. *Experimental mechanics* 35, (1995) 306–314.
- [10] H. Rossmann. Analysis of crack-tip Moiré fringe patterns. *International Journal of Fracture* 21, (1983) 83–106.
- [11] S. Ramaswamy, H. Tippur, and L. Xu. Mixed-mode crack-tip deformations studied using a modified flexural specimen and coherent gradient sensing. *Experimental mechanics* 33, (1993) 218–227.
- [12] Y. Kawagishi, M. Shozu, and Y. Hirose. Experimental evaluation of stress field around crack tip by caustic method. *Mechanics of materials* 33, (2001) 741–757.
- [13] R. J. Sanford. Determining fracture parameters with full-field optical methods. *Experimental Mechanics* 29, (1989) 241–247.

- [14] S. Yoneyama, Y. Morimoto, and M. Takashi. Automatic Evaluation of Mixed-mode Stress Intensity Factors Utilizing Digital Image Correlation. *Strain* 42, (2006) 21–29.
- [15] M. Carboni. Strain-gauge compliance measurements near the crack tip for crack closure evaluation: Applicability and accuracy. *Engineering fracture mechanics* 74, (2007) 563–577.
- [16] K. Ramesh, S. Gupta, and A. A. Kelkar. Evaluation of stress field parameters in fracture mechanics by photoelasticity revisited. *Engineering Fracture Mechanics* 56, (1997) 25–45.
- [17] A. K. S.N. Atluri. Mechanical responses of materials. A.S. Kobayashi (Ed.), Handbook on Experimental Mechanics, John Wiley & Sons, New York, 1993.
- [18] B. Pan, K. Qian, H. Xie, and A. Asundi. Two-dimensional digital image correlation for in-plane displacement and strain measurement: a review. *Measurement science and technology* 20, (2009) 062,001.
- [19] J. Yates, M. Zanganeh, R. Tomlinson, M. Brown, and F. D. Garrido. Crack paths under mixed mode loading. *Engineering Fracture Mechanics* 75, (2008) 319–330.
- [20] H. Sarangi, K. Murthy, and D. Chakraborty. Optimum strain gage locations for accurate determination of the mixed mode stress intensity factors. *Engineering Fracture Mechanics* 88, (2012) 63–78.
- [21] T. Chu, W. Ranson, and M. Sutton. Applications of digital-image-correlation techniques to experimental mechanics. *Experimental mechanics* 25, (1985) 232–244.
- [22] P. Lopez-Crespo, A. Shterenlikht, E. Patterson, J. Yates, and P. Withers. The stress intensity of mixed mode cracks determined by digital image correlation. *The Journal of Strain Analysis for Engineering Design* 43, (2008) 769–780.
- [23] P. Luo, Y. Chao, M. Sutton, and W. Peters III. Accurate measurement of three-dimensional deformations in deformable and rigid bodies using computer vision. *Experimental Mechanics* 33, (1993) 123–132.
- [24] G. Han, M. Sutton, and Y. Chao. A study of stationary crack-tip deformation fields in thin sheets by computer vision. *Experimental Mechanics* 34, (1994) 125–140.
- [25] S. Yoneyama, T. Ogawa, and Y. Kobayashi. Evaluating mixed-mode stress intensity factors from full-field displacement fields obtained by optical methods. *Engineering fracture mechanics* 74, (2007) 1399–1412.
- [26] A. A. Baker, L. F. Rose, and R. Jones. Advances in the bonded composite repair of metallic aircraft structure, volume 1. Elsevier, 2003.
- [27] R. Jones. Neutral axis offset effects due to crack patching. *Composite structures* 1, (1983) 163–174.
- [28] T. V. Umamaheswar and R. Singh. Modelling of a patch repair to a thin cracked sheet. *Engineering Fracture Mechanics* 62, (1999) 267–289.

- [29] A. C. Okafor, N. Singh, U. Enemuoh, and S. Rao. Design, analysis and performance of adhesively bonded composite patch repair of cracked aluminum aircraft panels. *Composite Structures* 71, (2005) 258–270.
- [30] C. N. Duong and C. H. Wang. Composite repair: theory and design. Elsevier, 2010.
- [31] M. Ayatollahi and R. Hashemi. Mixed mode Fracture in an inclined center crack repaired by composite patching. *Composite structures* 81, (2007) 264–273.
- [32] M. Ayatollahi and R. Hashemi. Computation of stress intensity factors (K I, K II) and T-stress for cracks reinforced by composite patching. *Composite structures* 78, (2007) 602–609.
- [33] M. Ramji and R. Srilakshmi. Design of composite patch reinforcement applied to mixed-mode cracked panel using finite element analysis. *Journal of Reinforced Plastics and Composites* 31, (2012) 585–595.
- [34] M. Ramji, R. Srilakshmi, and M. Bhanu Prakash. Towards optimization of patch shape on the performance of bonded composite repair using FEM. *Composites Part B: Engineering* 45, (2013) 710–720.
- [35] J. Poissant and F. Barthelat. A novel subset splitting procedure for digital image correlation on discontinuous displacement fields. *Experimental mechanics* 50, (2010) 353–364.
- [36] R. Zhu, H. Xie, Z. Hu, L. Jiang, B. Guo, and C. Li. Performances of different subset shapes and control points in subset-based digital image correlation and their applications in boundary deformation measurement. *Applied optics* 54, (2015) 1290–1301.
- [37] J. Chen, N. Zhan, X. Zhang, and J. Wang. Improved extended digital image correlation for crack tip deformation measurement. *Optics and Lasers in Engineering* 65, (2015) 103–109.
- [38] R.-c. Yang. A regularized finite-element digital image correlation for irregular displacement field. *Optics and Lasers in Engineering* 56, (2014) 67–73.
- [39] G. Yang, Z. Cai, X. Zhang, and D. Fu. An experimental investigation on the damage of granite under uniaxial tension by using a digital image correlation method. *Optics and Lasers in Engineering* 73, (2015) 46–52.
- [40] M. Eskandari, M. Yadegari-Dehnavi, A. Zarei-Hanzaki, M. Mohtadi-Bonab, R. Basu, and J. Szpunar. In-situ strain localization analysis in low density transformation-twinning induced plasticity steel using digital image correlation. *Optics and Lasers in Engineering* 67, (2015) 1–16.
- [41] H. Hosseini-Toudeshky, B. Mohammadi, and H. R. Daghyani. Mixed-mode fracture analysis of aluminium repaired panels using composite patches. *Composites science and technology* 66, (2006) 188–198.
- [42] H. HOSSEINI-TOUDESHPKY, B. Mohammadi, and S. Bakhshandeh. Mixed-mode fatigue crack growth of thin aluminium panels with single-side repair using experimental and numerical methods. *Fatigue & Fracture of Engineering Materials & Structures* 30, (2007) 629–639.

- [43] R. Srilakshmi, M. Ramji, and V. Chinthapenta. Fatigue crack growth study of CFRP patch repaired Al 2014-T6 panel having an inclined center crack using FEA and DIC. *Engineering Fracture Mechanics* 134, (2015) 182–201.
- [44] D.-C. Seo and J.-J. Lee. Fatigue crack growth behavior of cracked aluminum plate repaired with composite patch. *Composite Structures* 57, (2002) 323–330.
- [45] W.-Y. Lee and J.-J. Lee. Fatigue behavior of composite patch repaired aluminum plate. *Journal of composite materials* 39, (2005) 1449–1463.
- [46] G.-C. Tsai and S. B. Shen. Fatigue analysis of cracked thick aluminum plate bonded with composite patches. *Composite Structures* 64, (2004) 79–90.
- [47] T. Tay, F. Chau, and C. Er. Bonded boron-epoxy composite repair and reinforcement of cracked aluminium structures. *Composite structures* 34, (1996) 339–347.
- [48] J. Schubbe and S. Mall. Investigation of a cracked thick aluminum panel repaired with a bonded composite patch. *Engineering Fracture Mechanics* 63, (1999) 305–323.
- [49] D. Post. Moiré interferometry at VPI & SU. *Experimental Mechanics* 23, (1983) 203–210.
- [50] T. Dudderar and H. Gorman. The determination of mode I stress-intensity factors by holographic interferometry. *Experimental Mechanics* 13, (1973) 145–149.
- [51] P. K. Rastogi. Digital speckle pattern interferometry and related techniques. *Digital Speckle Pattern Interferometry and Related Techniques*, by PK Rastogi (Editor), pp. 384. ISBN 0-471-49052-0. Wiley-VCH, December 2000. 1.
- [52] Ncorr 2D-DIC Software. <http://www.ncorr.com>.
- [53] MATLAB. version 8.0 (R2012b). The MathWorks Inc., Natick, Massachusetts, 2012.
- [54] H. W. Schreier and M. A. Sutton. Systematic errors in digital image correlation due to under-matched subset shape functions. *Experimental Mechanics* 42, (2002) 303–310.
- [55] E. J. Williams and E. Williams. Regression analysis, volume 14. Wiley New York, 1959.
- [56] J. Fox and S. Weisberg. An R companion to applied regression. Sage, 2010.
- [57] T. L. Anderson. Fracture mechanics: fundamentals and applications. CRC press, 2005.
- [58] K. Naresh Reddy and M. Ramji. Material characterisation of Al-2014 T6 alloy using 3D-digital image correlation technique. *Proceedings of International conference on metallurgical and materials Processes, products and applications* .
- [59] G. P. Mogadpalli and V. Parameswaran. Determination of stress intensity factor for cracks in orthotropic composite materials using digital image correlation. *Strain* 44, (2008) 446–452.
- [60] H. Ramesh and M. Ramji. Adaptation of Open Source 2D DIC Software Ncorr for Solid Mechanics Applications. In 9th International Symposium on Advanced Science and Technology in Experimental Mechanics. 2014 .

- [61] R. Srilakshmi and M. Ramji. Experimental investigation of adhesively bonded patch repair of an inclined center cracked panel using DIC. *Journal of Reinforced Plastics and Composites* 33, (2014) 1130–1147.
- [62] N. R. Kolanu and M. Ramji. MATERIAL CHARACTERISATION OF AL-2014 T6 ALLOY USING 3D-DIGITAL IMAGE CORRELATION TECHNIQUE 2014.
- [63] M. Kashfuddoja and M. Ramji. Critical analysis of adhesive layer behavior in patch-repaired carbon fiber-reinforced polymer panel involving digital image correlation. *Journal of Composite Materials* 0021998314541312.
- [64] M. Kashfuddoja, R. Prasath, and M. Ramji. Study on experimental characterization of carbon fiber reinforced polymer panel using digital image correlation: A sensitivity analysis. *Optics and Lasers in Engineering* 62, (2014) 17–30.
- [65] J. Blaber, B. Adair, and A. Antoniou. Ncorr: Open-source 2D digital image correlation Matlab software. *Experimental Mechanics* 1–18.
- [66] S. Atluri and A. Kobayashi. Mechanical responses of materials. *VCH Publishers, Inc., Handbook on Experimental Mechanics. Second Revised Edition(USA), 1993*, 1–37.
- [67] S. Yoneyama, T. Ogawa, and Y. Kobayashi. Evaluating mixed-mode stress intensity factors from full-field displacement fields obtained by optical methods. *Engineering fracture mechanics* 74, (2007) 1399–1412.